SAND REPORT
SAND2002-2425
Unlimited Release
Printed August 2002

The Implementation of Braided Composite Materials in the Design of a Bend-Twist Coupled Blade

James Locke and Ivan Contreras Hidalgo
Wichita State University
Department of Aerospace Engineering
Wichita, Kansas 67260

Prepared by
Sandia National Laboratories
Albuquerque, New Mexico 87185 and Livermore, California 94550

Sandia is a multiprogram laboratory operated by Sandia Corporation, a Lockheed Martin Company, for the United States Department of Energy under Contract DE-AC04-94AL85000.

Sandia National Laboratories

Issued by Sandia National Laboratories, operated for the United States Department of Energy by Sandia Corporation.

Available to DOE and DOE contractors from
U.S. Department of Energy
Office of Scientific and Technical Information
P.O. Box 62
Oak Ridge, TN 37831

Telephone: (865)576-8401
Facsimile: (865)576-5728
E-Mail: reports@adonis.osti.gov
Online ordering: http://www.doe.gov/bridge

Available to the public from
U.S. Department of Commerce
National Technical Information Service
5285 Port Royal Rd
Springfield, VA 22161

Telephone: (800)553-6847
Facsimile: (703)605-6900
E-Mail: orders@ntis.fedworld.gov
Online order: http://www.ntis.gov/ordering.htm

SAND2002-2425
Unlimited Release
Printed August 2002

The Implementation of Braided Composite Materials in the Design of a Bend-Twist Coupled Blade

James Locke and Ivan Contreras Hidalgo
(*Associate Professor and Graduate Research Assistant*)
Wichita State University
Department of Aerospace Engineering
Wichita, Kansas 67260-0044

Abstract

This report presents results for conceptual wind turbine blade designs that are manufactured using braided composite materials. The SERI-8 wind turbine blade was used to define a geometric model and establish the blade internal volume as well as the primary load-carrying box beam structure. The box beam was modeled in twelve pieces and characterized by its principal dimensions (height, width, and perimeter) at the different cross-sectional areas along the span of the blade. A composite beam theory model was used to parametrically evaluate design candidates. The bending stiffness of the SERI-8 blade was used as a constraint (or match parameter), and the wall thickness and twist angle results as the performance parameters. Internal loads were also computed as part of the parametric study. A design was chosen according to the more favorable parameters, and a detailed analysis was made in terms of braided composite final arrangement, number of braided preforms (or socks), wall thickness, induced twist angle, and internal loads. To evaluate the relative accuracy of the beam model, beam twist results were compared with finite element twist results. These preliminary results indicate that a braided composite box structure can be designed with the required stiffness properties and a high level of structural coupling.

Acknowledgments

This project was supported by Sandia National Laboratories under Standard Purchase Order No. 21629. The technical monitor was Thomas Ashwill. The authors would like to thank Thomas Ashwill and Paul Veers for their guidance and support.

This is a Contractor Report for Sandia National Laboratories that partially fulfills the deliverables under Contract #21629.

TABLE OF CONTENTS

LIST OF FIGURES

LIST OF TABLES

1 INTRODUCTION

The main purpose of this investigation is to study the feasibility of using braided composite preforms to manufacture a wind turbine blade with adequate structural integrity and bend-twist coupling. An example braided preform is shown in Figure 1a, and an example of the results that can be achieved with braided composites and Resin Transfer Molding (RTM) is shown in Figure 1b. A key advantage in using braided preforms is the relative ease of manufacturing compared to conventional laminated composites. Moreover, the structural box is continuous, and fatigue/damage tolerance performance is better than conventional laminated composites [1].

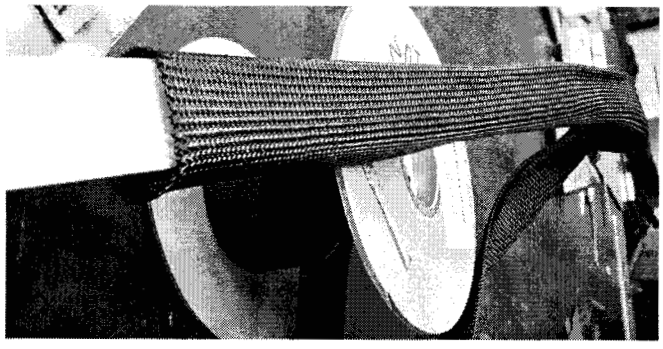

Figure 1a: Braided preform

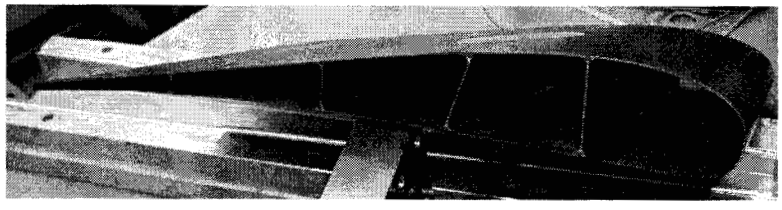

Figure 1b: 2D biaxial braided wing control surface via RTM

Wind turbine blades carry loads primarily by bending and twisting. Coupling between bending and twisting can be used to reduce extreme loads and improve fatigue performance. Incremental loads (with respect to a given steady state condition) are reduced because when the blade deforms in bending the bend-twist coupling produces a decrease in the blade twist (and angle of attack). The level of load reduction depends on the twist distributed along the blade length, which is controlled by the level of bend-twist coupling. The level of bend-twist coupling depends on the blade cross-sectional geometry, the level of anisotropy in the structural material, and the material distribution.

For conventional laminated composites constructed of orthotropic layers, the level of anisotropy (extensional-shear coupling) is determined by the fiber orientation with respect

to the primary loading direction. Fibers oriented at an angle θ, as shown in Figure 2, can be used to produce either bend-twist coupling or extensional-twist coupling. Bend-twist coupling requires the mirror lay-up shown in Figure 2(a).

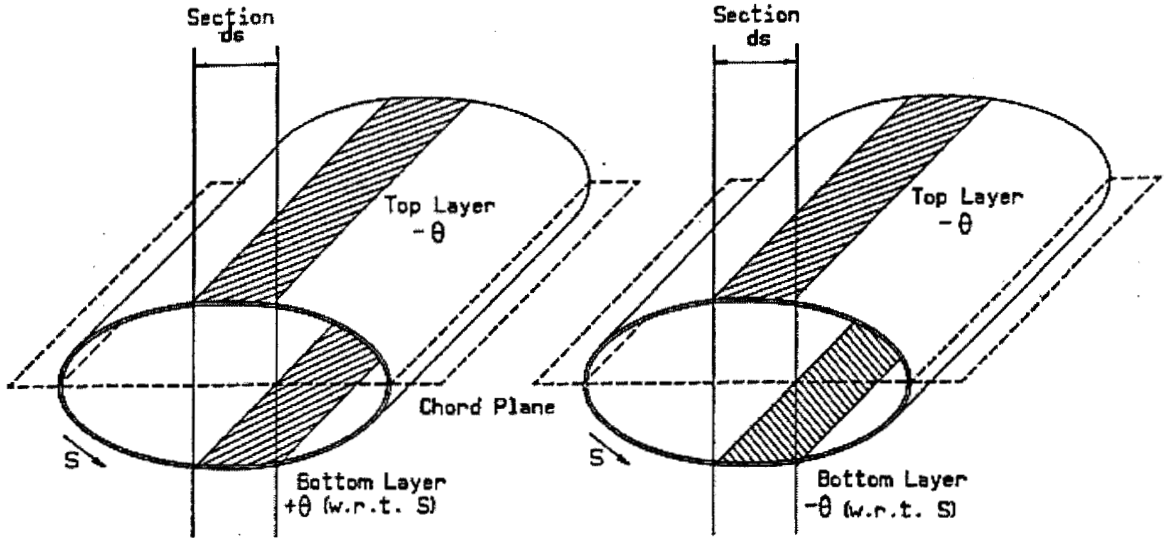

(a) "Mirror" lay-up for bending/twisting coupling (θ changes sign below chord)

(b) "Helical" lay-up for stretching/twisting coupling (θ has same sign around S)

Figure 2: Lay-up for bend-twist and stretch-twist coupling

The use of one braided preform would produce the helical lay-up (with extensional-twist coupling) shown in Figure 2(b). Thus, for bend-twist coupling a single preform must be cut and used in two halves to achieve a mirror lay-up. Alternatively, two (or more) preforms can be used to manufacture the box structures shown in Figure 3.

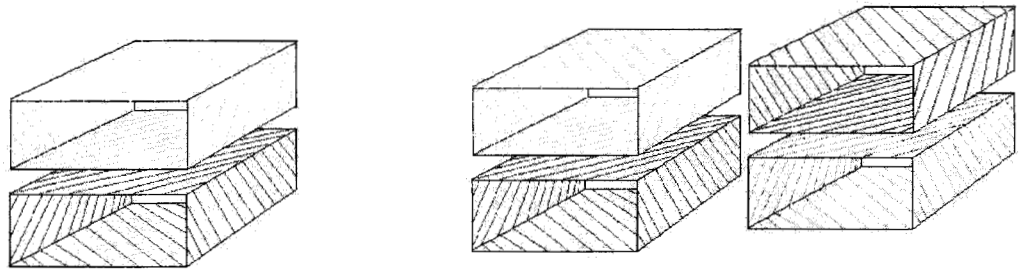

Figure 3: Braided composite arrangement for a bend-twist coupled structure

2 DESIGN CONCEPTS

Based on the designs shown in Figure 3, four candidate design concepts were selected as shown in Figure 4. Common features of all proposed designs are:

- Tape plies can be added to vertical webs and spar caps as required to achieve required stiffnesses and bend-twist coupling
- Braided preform wrapped around entire box
- Leading and trailing edges foam filled
- Braided preform wrapped around entire blade cross-section
- Foam between spar caps and outer surface for added buckling resistance

Design details are listed as follows:

(a) Single Box (SB) with Horizontal Web, and (b) Double Box (DB) with Horizontal Web

- Boxes manufactured using continuous braided preforms with no cuts

(c) Single Box without Horizontal Web, and (d) Double Box without Horizontal Web

- Upper and lower box sections manufactured using braided preforms that are wrapped around a mandril for the entire box and cut in half
- Mirror lay-up to achieve the desired coupling

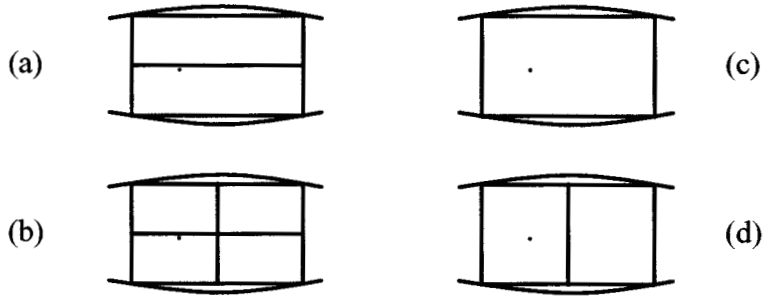

Figure 4: Candidate design concepts

The first design concept (a) is the coupled double box proposed by de Goeij et. al. [2]. This type of structure circumvents the well known problems of traditional construction, namely joint strain incompatibilities and de-bond due to the poor adhesive characteristics. Based on these findings, it would be desirable to use 2D braided composite to construct an integral closed structure with the desired stiffness and bend-twist coupling. Concept (b) is a variation of (a) that has the same basic characteristics and more bending stiffness, due to the added vertical web. This concept also reduces the internal loads and stresses by shifting load from the outer vertical webs to the inside vertical web. Concepts (c) and (d), respectively, have the same stiffness properties as (a) and (b), respectively. The main

difference between these concepts is the manufacturing method. Concepts (a) and (b) can be manufactured using continuous braided performs with no cuts. Concepts (c) and (d) require separate halves that must be spliced together with additional plies. A detailed analysis model is required to quantify the increase in weight and internal stresses due to these additional plies. It is estimated that the added weight will be approximately equal to the horizontal web weight of concepts (a) and (b). Furthermore, concepts (c) and (d) will be more difficult to manufacture. Based on these considerations, concepts (c) and (d) will not be considered further. Only concepts (a) and (b) will be considered in detail. These concepts are referred to as Single Box (SB) for concept (a) and Double Box (DB) for concept (b).

3 GEOMETRIC MODEL

To evaluate the performance of each design concept, an approximate box beam model was constructed based on the SERI-8 blade dimensions given by Ong & Tsai [3]. Since the model was set up to evaluate only the blade, the root fitting is not included. The resulting idealized model is shown in Figure 5.

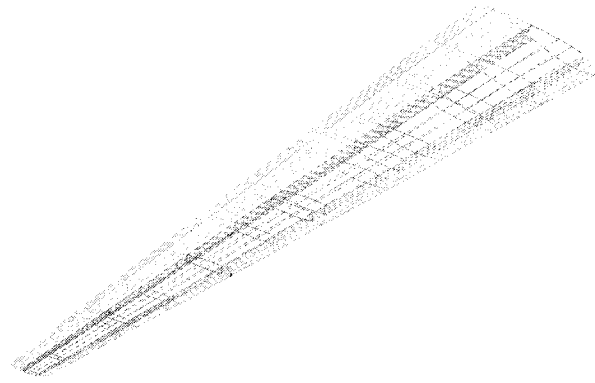

Figure 5: SERI-8 Blade Model [3] STA 60 to STA 312

Starting with the blade geometric model shown in Figure 5, base box beam dimensions were determined at each blade station. The base dimensions (listed in Table 1) consist of the height at each spar location, the width (or chord), and the box perimeter. These base dimensions were then approximated by idealizing the two curved walls at the top and bottom of the box as straight line segments and calculating an average height value at each blade station. The resulting principal dimensions (height, width, and perimeter) of each cross-sectional area are listed in Table 2. Since the 12 piecewise partitions do not permit a smooth property variation, the principal box dimensions were linearized as shown in Table 3 and Figures 6 and 7.

STA	REAR SPAR [in]	UPPER LEFT SKIN [in]	LOWER LEFT SKIN [in]	MIDDLE SPAR [in]	UPPER RIGHT SKIN [in]	LOWER RIGHT SKIN [in]	FRONT SPAR [in]	PERIMETER CELL 1 [in]	PERIMETER CELL2 [in]	PERIMETER OF THE OUTER BOUNDARY [in]
60	6.138	8.841	8.975	8.752	8.820	8.803	8.448	32.706	34.822	50.025
84	6.011	8.658	8.790	8.571	8.638	8.621	8.273	32.029	34.102	48.990
108	5.248	8.316	8.393	7.323	8.291	8.312	6.424	29.280	30.350	44.984
132	4.976	7.884	7.957	6.943	7.861	7.872	6.091	27.760	28.766	42.640
156	4.651	7.370	7.438	6.490	7.348	7.366	5.694	25.950	26.899	39.868
180	4.192	6.779	6.787	5.251	6.778	6.777	4.334	23.009	23.140	35.648
204	3.796	6.137	6.144	4.754	6.136	6.136	3.924	20.831	20.950	32.274
228	3.364	5.440	5.446	4.213	5.439	5.438	3.478	18.463	18.568	28.605
252	2.838	4.683	4.676	3.128	4.703	4.683	2.371	15.325	14.885	23.954
276	2.239	3.882	3.880	2.390	3.903	3.883	1.812	12.391	11.988	19.599
300	1.660	3.038	3.038	1.710	3.056	3.639	1.297	9.447	9.703	15.729
312	1.420	2.600	2.600	1.464	2.615	2.601	1.110	8.084	7.790	12.947

Table 1: Box beam base model

STA	REAR SPAR [in]	UPPER LEFT SKIN [in]	LOWER LEFT SKIN [in]	MIDDLE SPAR [in]	UPPER RIGHT SKIN [in]	LOWER RIGHT SKIN [in]	FRONT SPAR [in]	PERIMETER CELL 1 [in]	PERIMETER CELL2 [in]	PERIMETER OF THE OUTER BOUNDARY [in]
60	7.779	8.810	8.810	7.779	8.810	8.810	7.779	33.178	33.178	50.798
84	7.618	8.630	8.630	7.618	8.630	8.630	7.618	32.497	32.497	49.757
108	6.332	8.290	8.290	6.332	8.290	8.290	6.332	29.243	29.243	45.823
132	6.003	7.860	7.860	6.003	7.860	7.860	6.003	27.726	27.726	43.446
156	5.612	7.350	7.350	5.612	7.350	7.350	5.612	25.923	25.923	40.623
180	4.593	6.760	6.760	4.593	6.760	6.760	4.593	22.705	22.705	36.225
204	4.158	6.120	6.120	4.158	6.120	6.120	4.158	20.556	20.556	32.796
228	3.685	5.420	5.420	3.685	5.420	5.420	3.685	18.210	18.210	29.050
252	2.779	4.670	4.670	2.779	4.670	4.670	2.779	14.898	14.898	24.238
276	2.147	3.880	3.880	2.147	3.880	3.880	2.147	12.054	12.054	19.814
300	1.556	3.030	3.030	1.556	3.030	3.030	1.556	9.172	9.172	15.232
312	1.331	2.600	2.600	1.331	2.600	2.600	1.331	7.863	7.863	13.063

Table 2: Approximate box beam model

PROPERTIES		STA 60	STA 84	STA 108	STA 132	STA 156	STA 180	STA 204	STA 228	STA 252	STA 276	STA 300	STA 312
Box Beam Model I													
Single Box													
Height (H)	[in]	7.915	7.283	6.652	6.021	5.390	4.759	4.127	3.496	2.865	2.234	1.603	1.287
Width (W)	[in]	18.910	17.686	16.462	15.238	14.014	12.790	11.566	10.342	9.118	7.894	6.670	6.058
Perimeter (P_g)	[in]	53.654	49.946	46.238	42.53	38.822	35.114	31.406	27.698	23.99	20.282	16.574	14.72
Box Beam Model II													
Double Box (Vert. Web)													
cell 1		**STA 60**	**STA 84**	**STA 108**	**STA 132**	**STA 156**	**STA 180**	**STA 204**	**STA 228**	**STA 252**	**STA 276**	**STA 300**	**STA 312**
Height (H)	[in]	7.9146	7.2834	6.6522	6.021	5.3898	4.7586	4.1274	3.4962	2.865	2.2338	1.6026	1.287
Width (W)	[in]	9.455	8.843	8.231	7.619	7.007	6.395	5.783	5.171	4.559	3.947	3.335	3.029
Perimeter (P_g)	[in]	34.739	32.2526	29.7662	27.2798	24.7934	22.307	19.8206	17.3342	14.8478	12.3614	9.875	8.6318
cell 2		**STA 60**	**STA 84**	**STA 108**	**STA 132**	**STA 156**	**STA 180**	**STA 204**	**STA 228**	**STA 252**	**STA 276**	**STA 300**	**STA 312**
Height (H)	[in]	7.9146	7.2834	6.6522	6.021	5.3898	4.7586	4.1274	3.4962	2.865	2.2338	1.6026	1.287
Width (W)	[in]	9.455	8.843	8.231	7.619	7.007	6.395	5.783	5.171	4.559	3.947	3.335	3.029
Perimeter (P_g)	[in]	34.739	32.2526	29.7662	27.2798	24.7934	22.307	19.8206	17.3342	14.8478	12.3614	9.875	8.6318
Box Beam Model III													
Double Box (Horzt. Web)													
cell 1		**STA 60**	**STA 84**	**STA 108**	**STA 132**	**STA 156**	**STA 180**	**STA 204**	**STA 228**	**STA 252**	**STA 276**	**STA 300**	**STA 312**
Height (H)	[in]	3.9543	3.6375	3.3207	3.0039	2.6871	2.3703	2.0535	1.7367	1.4199	1.1031	0.7863	0.6279
Width (W)	[in]	18.91	17.686	16.462	15.238	14.014	12.79	11.566	10.342	9.118	7.894	6.67	6.058
Perimeter (P_g)	[in]	45.74	42.6632	39.5864	36.5096	33.4328	30.356	27.2792	24.2024	21.1256	18.0488	14.972	13.4336
cell 2		**STA 60**	**STA 84**	**STA 108**	**STA 132**	**STA 156**	**STA 180**	**STA 204**	**STA 228**	**STA 252**	**STA 276**	**STA 300**	**STA 312**
Height (H)	[in]	3.9543	3.6375	3.3207	3.0039	2.6871	2.3703	2.0535	1.7367	1.4199	1.1031	0.7863	0.6279
Width (W)	[in]	18.91	17.686	16.462	15.238	14.014	12.79	11.566	10.342	9.118	7.894	6.67	6.058
Perimeter (P_g)	[in]	45.74	42.6632	39.5864	36.5096	33.4328	30.356	27.2792	24.2024	21.1256	18.0488	14.972	13.4336

Table 3: Approximate box beam model linearized geometric parameters

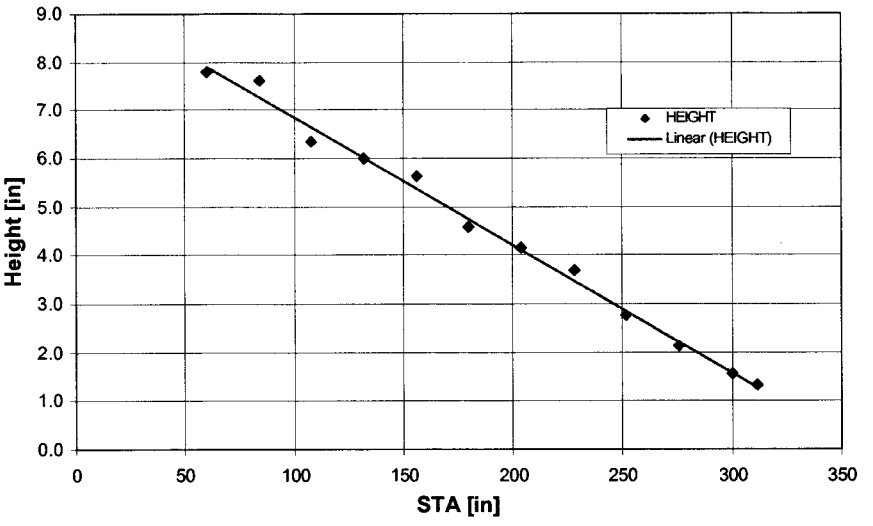

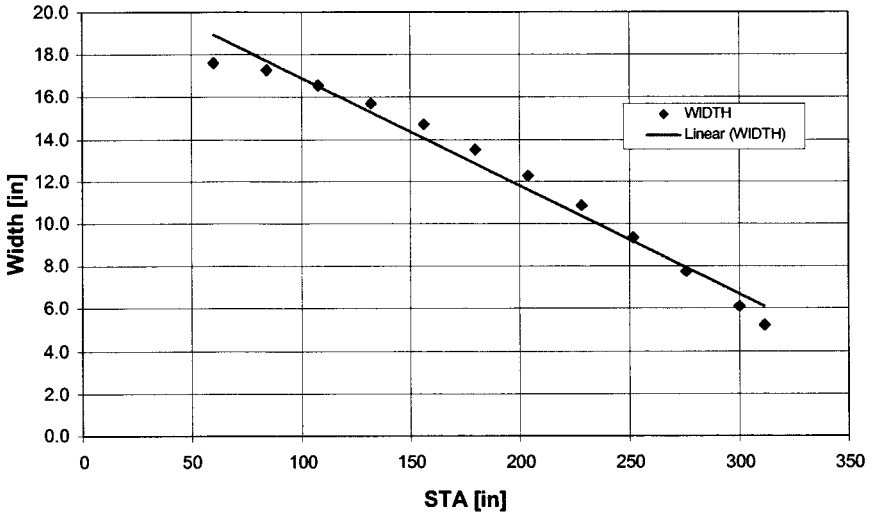

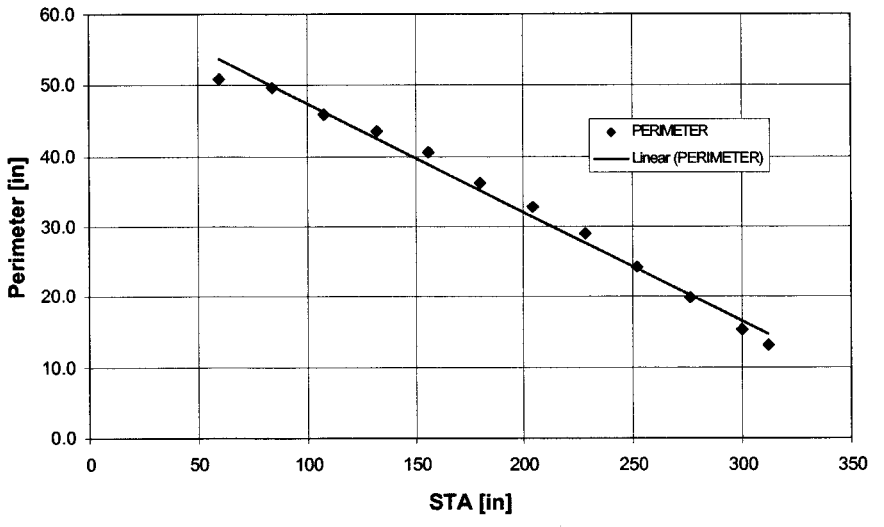

Figure 6: Single box geometric parameters

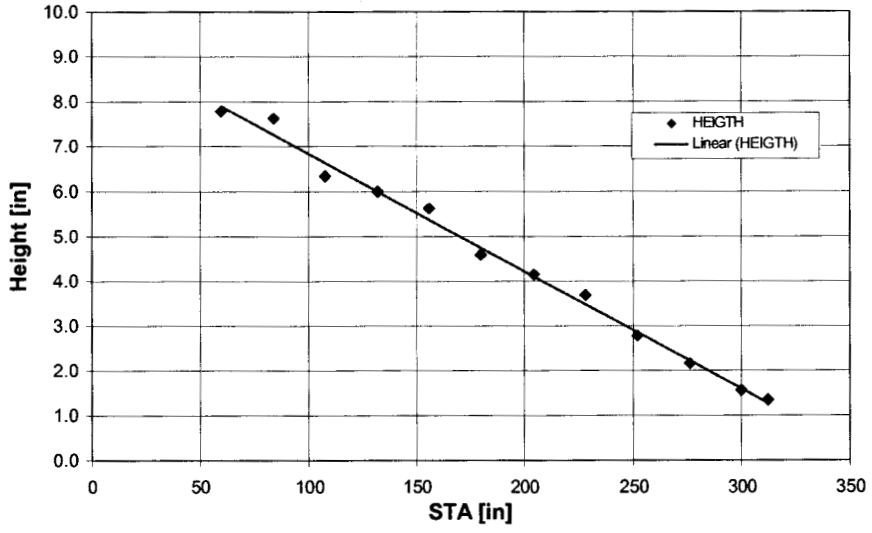

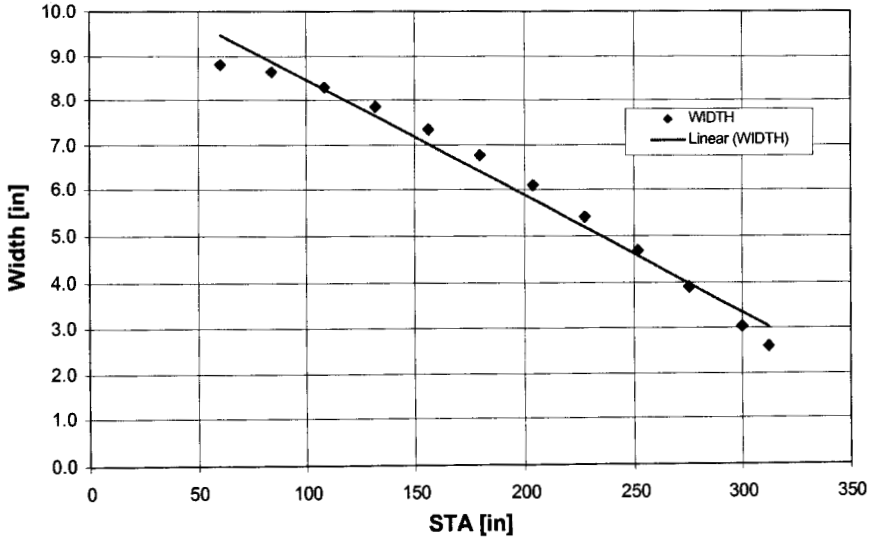

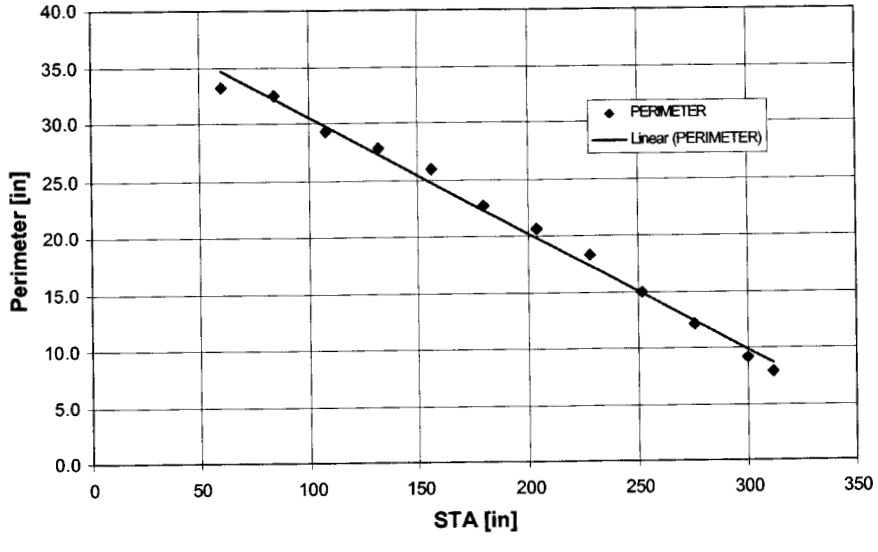

Figure 7: Double box geometric parameters

4 BRAIDED COMPOSITES

Traditional braiding involves a series of yarn carriers that follow intersecting circular paths so that the yarns interlace to form a tubular fabric as shown in Figure 1. A typical 2D braider is illustrated in Figure 8a [4]. An actual braider is shown in Figure 8b. A mandrel that passes through the braider may be used to control the final fabric configuration. The rotational speed of the yarn carriers relative to the transverse speed of the mandrel controls the orientation of the yarns. The mandrel can vary in cross-section, with the braided fabric conforming to the mandrel shape. A standard sock braided composite is usually defined by its initial braid angle θ in degrees (usually 45) and its initial perimeter P_θ. For a given perimeter, the sock can be stretched (decreasing the perimeter) or compressed (increasing the perimeter) in order to fit a particular shape. The variation in perimeter with respect to the initial perimeter changes the braid angle. Thus, the braid angle is a function of the taper geometry for a tapered box beam. Using this property, it is possible to select a variety of socks with different initial perimeters at 45 degrees that will fit a tapered box beam.

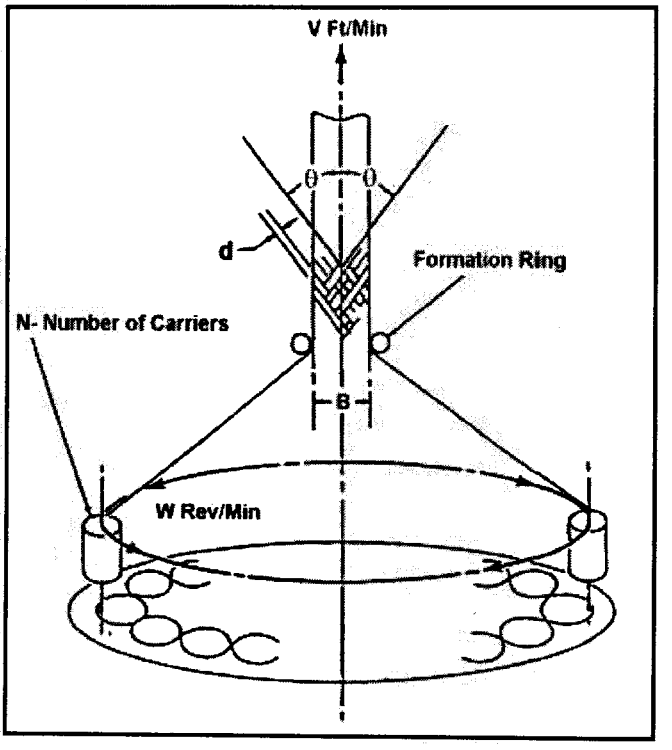

Figure 8a Maypole braider for production of 2D bias braid [4]

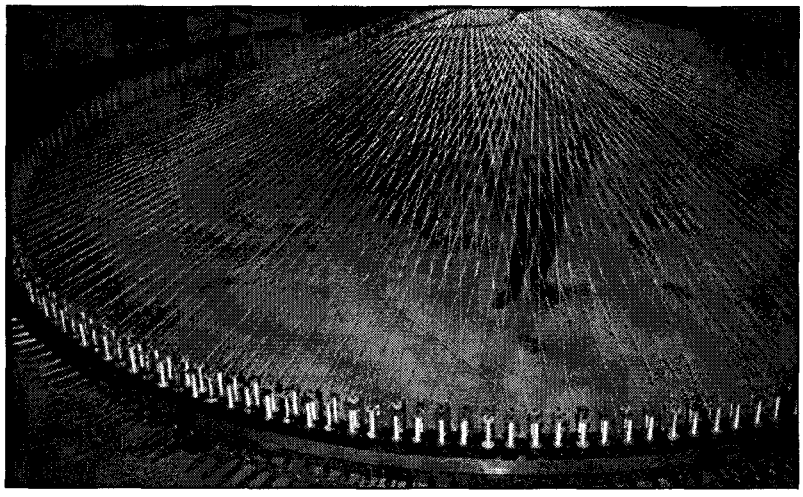

Figure 8b Braider for production of 2D preforms

According to reference 5 a range between 15 and 30 degrees permits a favorable bend-twist coupling with the highest coupling coefficient at 20 degrees. Several braided composite models were generated in order to study the maximum and minimum angles generated by the different design concepts (tapered beams); three of them (Figures 9a, b, c), were modeled and chosen for the parametric study. Results were also obtained for an ideal base model with a constant 20 degree braid angle. For each of the cases a different initial braided sock is stretched over the tapered beam mandrel in order to obtain the shown angle variation. As shown in the Figures, the models were set up to achieve 20 degrees at different zones of the rotor blade: 20 @ STA 84, 20 @ STA 156 and 20 @ STA 228.

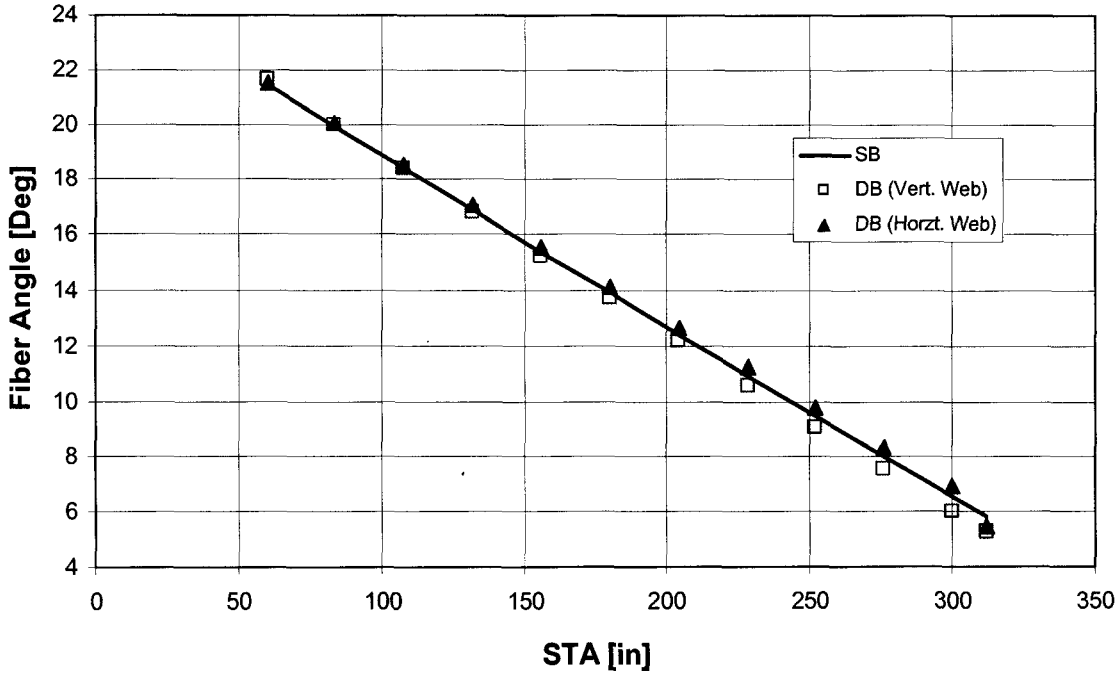

Figure 9a: 20 Degree Braid Angle achieved at STA 84

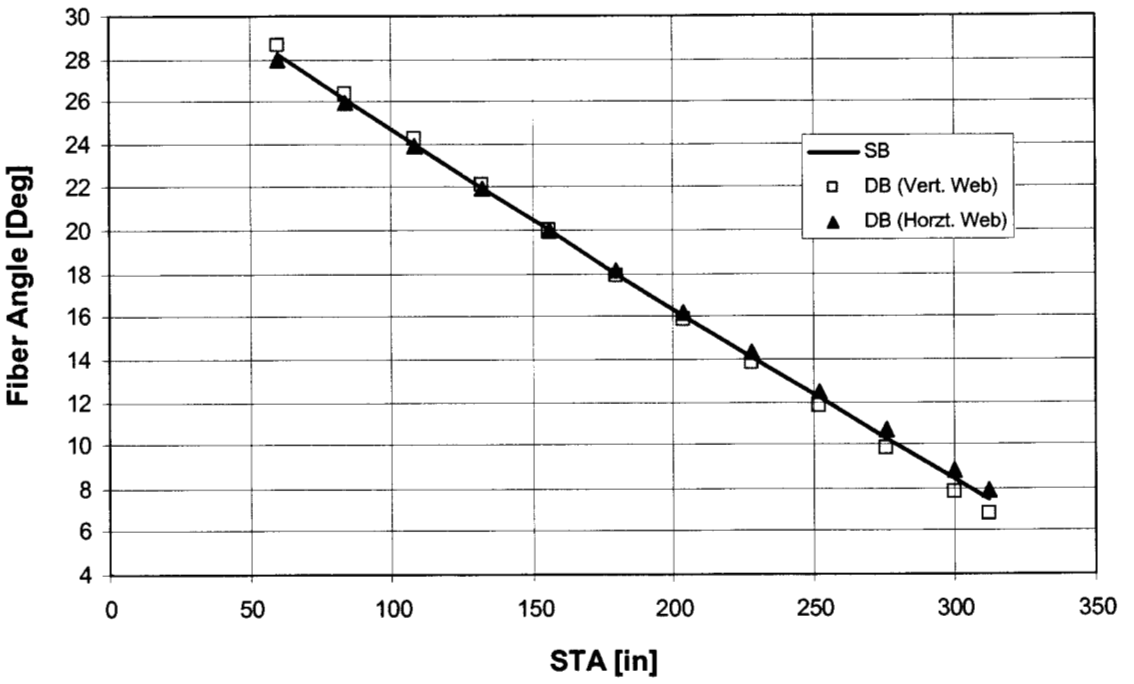

Figure 9b: 20 Degree braid angle achieved at STA 156

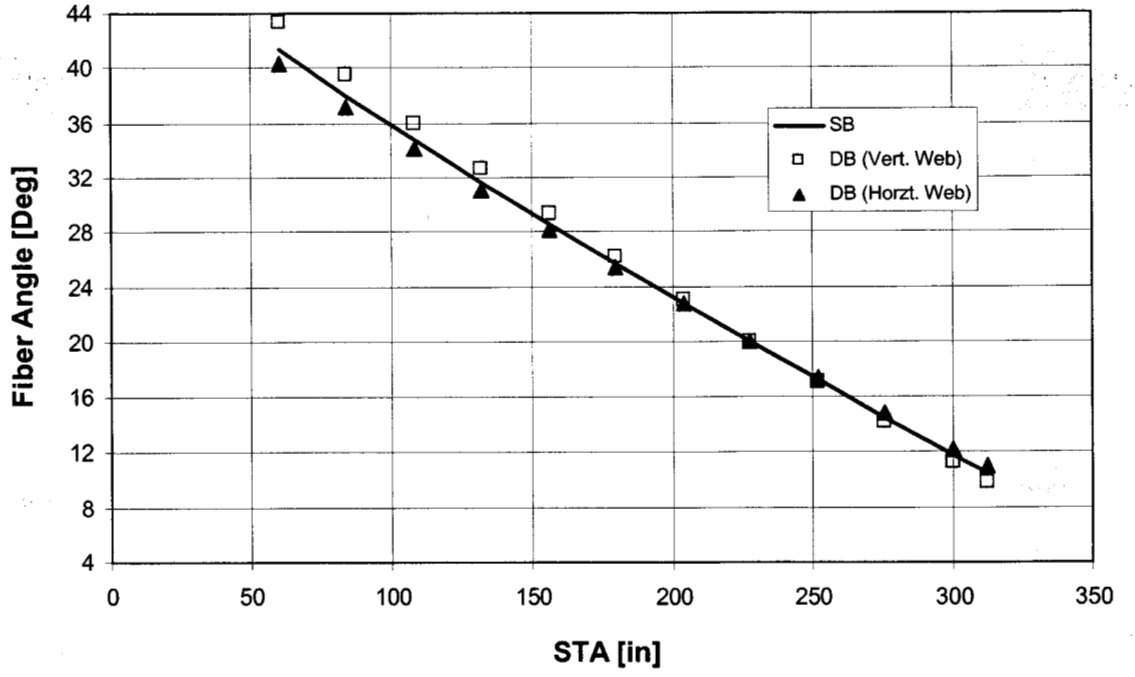

Figure 9c: 20 Degree braid angle achieved at STA 228

5 MATHEMATICAL MODEL

The beam models used for this study are based on the single-cell thin-walled anisotropic beam theory presented by Libove [6]. For this study, the theory was extended to two-cell boxes by making appropriate additions to the governing equations. Key assumptions for the theory are listed as follows:

1. The method assumes that the shape of the cross sections is preserved, thereby neglecting Poisson's ratio effects.

2. The beam segments are assumed to be subjected to an equilibrium system of external loads consisting only of forces and couples applied to the end cross sections as concentrated loads. Consequently, the forces and torque are constant along the length of a given beam segment. In order for the present theory to apply, distributed loadings must be approximated by concentrated forces and couples at discrete cross sections.

3. The walls are assumed to be thin enough to be regarded as membranes in plane stress. In addition, the normal stress resultant in the circumferential direction is assumed to be negligible, so that the state of stresses at any point can be described by a shear flow, q, and a longitudinal axial force, N, as shown in Figure 10.

4. The shear flow is constant along the length of a beam segment.

5. Longitudinal strain is a linear function of the cross-sectional coordinates, x and y, shown in Figure 11.

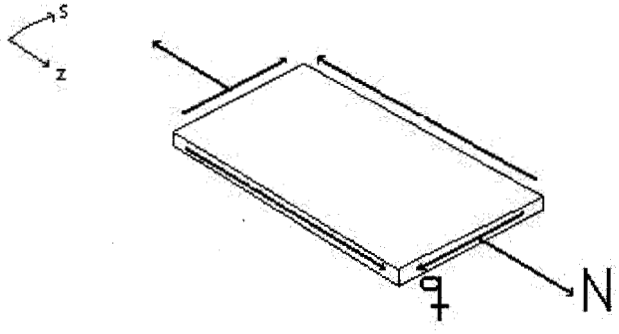

Figure 10: State of plane stress with shear flow and axial force

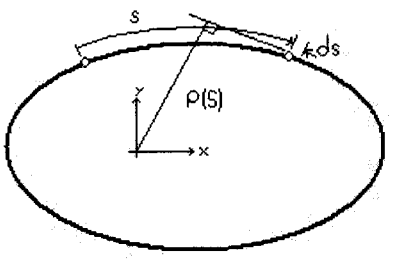

Figure 11: Thin-walled beam cross-section

The membrane forces developed in the beam walls are given by classical lamination theory as follows:

$$\begin{Bmatrix} N \\ N_s \\ q \end{Bmatrix} = [A] \begin{Bmatrix} \varepsilon \\ \varepsilon_s \\ \gamma \end{Bmatrix} \qquad (1)$$

where $[A]$ is the membrane stiffness matrix. Using the third assumption ($N_s = 0$) the equations relating forces and strains can be written as follows:

$$\begin{aligned} N &= \beta_1 \varepsilon + \beta_2 q \\ \gamma &= -\beta_2 \varepsilon + \beta_4 q \end{aligned} \qquad (2)$$

where the beta terms are defined as

$$\begin{aligned} \beta_1 &= A_{11} - \frac{{A_{12}}^2}{A_{22}} - \frac{{\beta_2}^2}{\beta_4} \\ \beta_2 &= \left(A_{16} - \frac{A_{12} A_{26}}{A_{22}} \right) \beta_4 \\ \beta_4 &= \left(A_{66} - \frac{{A_{26}}^2}{A_{22}} \right)^{-1} \end{aligned} \qquad (3)$$

The fifth assumption states that the longitudinal strain is a linear function of the cross-sectional coordinates. Thus, the axial force can be expressed as:

$$N = \beta_1 \varepsilon + \beta_2 q \qquad \text{where} \qquad \varepsilon = \varepsilon_0 - y\kappa_x - x\kappa_y \qquad (4)$$

Static equivalence of the wall stresses with the cross-sectional stress resultants produces the following equations relating the bending moment, M_x, and torsion, T, to the bending curvature, κ_x, and rate of twist, ϕ_z:

$$\begin{Bmatrix} M_x \\ T \end{Bmatrix} = \begin{bmatrix} EI & -\beta GJ \\ -\beta GJ & GJ \end{bmatrix} \begin{Bmatrix} \kappa_x \\ \phi_z \end{Bmatrix} \qquad (5)$$

where EI is the bending stiffness, GJ is the torsional stiffness, and β is a coupling parameter that is proportional to the beam cross-sectional geometry and the material coupling constant β_2.

Using the notation of reference 7, Eq. (5) can be expressed as

$$\begin{Bmatrix} M_x \\ T \end{Bmatrix} = \begin{bmatrix} EI & -g \\ -g & GJ \end{bmatrix} \begin{Bmatrix} \kappa_x \\ \phi_z \end{Bmatrix} \qquad (6)$$

where the level of coupling is defined in terms of the coupling coefficient

$$\alpha = \frac{g}{\sqrt{EI \cdot GJ}} \qquad (7)$$

Comparing Eqs. (5) and (6), the coupling term, g, is equal to βGJ. Substituting this value into Eq. (7) yields the following relationship between the two coefficients α and β:

$$\beta = \alpha\sqrt{EI/GJ} \qquad (8)$$

For this study, the SB and DB design concepts were analyzed for the elastic constant distributions shown in Figure 12.

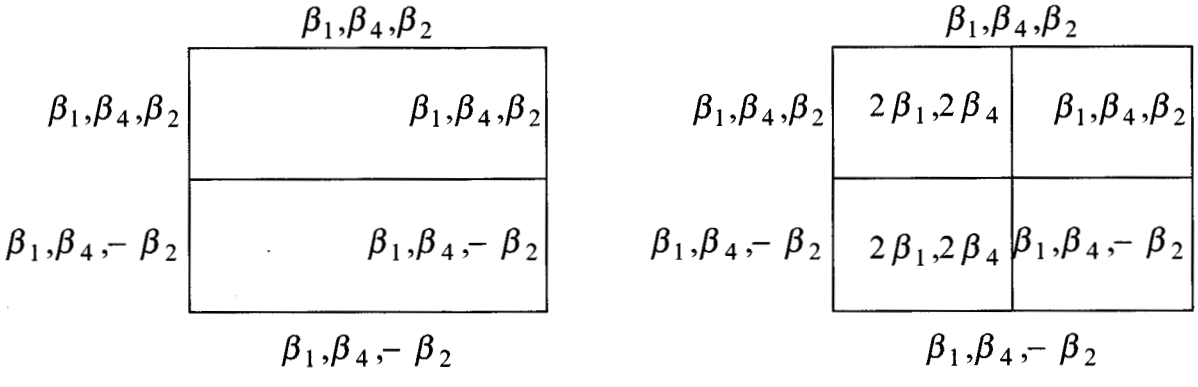

Figure 12: (a) Single box and (b) double box cross-section elastic constant distribution

These distributions produce the desired bend-twist coupling. Since the upper and lower halves of the boxes are mirror images of each other, the elastic constants β_1 and β_4 will continue to be constant throughout the cross section, but β_2 will change sign from the upper half to the lower half. The stiffness terms for these designs are given as follows:

$$GJ = \frac{2a^2b^2}{\beta_4(a+b)} \qquad \beta = \frac{\beta_2}{2}\left(1+\frac{b}{2a}\right)$$
$$EI = EI_0 + \beta^2 GJ \qquad a = \text{width} \quad b = \text{height}$$

where (9)

$$EI_0 = \beta_1\left(\frac{b^3}{6}+\frac{ab^2}{2}\right) \text{ for the single box}$$

$$EI_0 = \beta_1\left(\frac{b^3}{3}+\frac{ab^2}{2}\right) \text{ for the double box}$$

Thus, the level of coupling is directly proportional to the material constant β_2.

The design approach utilized for the present study was based on using Eqs. (9) to determine the stiffness terms and Eq. (8) to determine the level of coupling. Designs that produced the required level of stiffness combined with a high level of coupling were identified based on parametric studies.

An alternative design approach could have been utilized if more design information were available. The alternative approach requires a bending deflection distribution, a twist distribution, and a bending moment distribution. Given these inputs, the required bending stiffness, $EI_{0_{req}}$, and coupling parameter, β_{req}, for a given bending curvature and rate of twist are given as

$$EI_{0_{req}} = \frac{M_x}{\kappa_x} \qquad \beta_{req} = \frac{EI_{0_{req}}}{M_x}\phi_z = \frac{\phi_z}{\kappa_x} \qquad (10)$$

These equations can be used to design for the desired levels of bending deflection and twist.

6 PARAMETRIC STUDY

All results are based on using the following material properties:

Carbon weave: $E_1 = 20\times10^6$ psi, $E_2 = 1.3\times10^6$ psi, $G_{12} = 1.03\times10^6$ psi, $\nu_{12} = 0.3$

Glass weave: $E_1 = 6\times10^6$ psi, $E_2 = 1.26\times10^6$ psi, $G_{12} = 0.6\times10^6$ psi, $\nu_{12} = 0.3$

Initially, the DB and SB designs were sized to match the bending stiffness of the SERI-8 blade [3], see Figure 13. According to previous studies [2, 5, 7], a range between 30 and 15 degrees produces a favorable bending-twist coupling with the highest coupling coefficient at 20 degrees. Several braided composite models were generated in order to study the maximum and minimum angles generated by the different design concepts. These models were designed to achieve 20 degrees at different zones of the blade (20 degrees @ STA 84, 20 degrees @ STA 156, and 20 degrees @ STA 228). For comparison purposes, a baseline model with a constant 20 degree angle was also studied. The required box thickness for the SB and DB concepts is shown in Figure 14. These thickness values have been determined based on a uniform wall thickness at a given station for each box. Note that the design with 20 degrees @ STA 228 requires more material to achieve the desired stiffness. This model is excluded from further consideration.

To evaluate the twist angle and internal loads the boxes were loaded with the discrete point loads from reference 3, which corresponds to an equivalent wind speed of 70 m/s and a C_d of 1.7. A comparison of the DB and SB concepts is shown in Figures 15 through 17. Box thickness values are shown in Figure 15; twist angle is shown in Figure 16; internal loads are shown in Figure 17. The twist angle values are unusually large for two reasons. First, the initial parametric studies were conducted assuming that all braided fibers were high modulus carbon in one weave direction with no fibers in the other weave direction. This is not realistic and will be addressed later. Second, no pre-twist was included in the analysis. Therefore, the twist angle values shown in Figure 16 should be viewed as relative (not absolute) values. The coupling coefficient values vary according to the braid angle. As indicated, the coupling coefficient values are comparable with those obtained in previous studies [5, 7]. The SB design has a slightly higher coupling coefficient than the DB design.

The two design concepts require essentially the same thickness. The DB concept requires a slightly smaller thickness value, but will have more material due to the additional vertical web. Twist angle values are also close with a difference of about 5%. The SB concept produces the most twist. Internal loads differ more than the thickness or the twist. The SB shear flow at STA 60 is 48% higher than the DB value, and the SB axial force is 15% higher than the DB value. The DB design (with the additional vertical web) is also more resistant to buckling and provides multiple redundancy. Therefore, the DB concept is judged to be the most promising design, and the SB concept is excluded from further consideration.

The undulating thickness variations shown in Figures 14 and 15 would be very difficult (and undesirable) to manufacture. The main problem is that more material layers are

required at the tip with fewer at the mid section and more at the root of the blade. A more efficient design is achieved if a few continuous layers of material are used. Three linear thickness profiles were used to investigate the effect of thickness variation. These profiles (labeled t1, t2 and t3) are shown in Figure 18. Stiffness and twist angle values are shown in Figures 19 and 20. With the exception of the tip area stiffness, all of the thickness profiles result in stiffness variations that meet or exceed the SERI-8 stiffness. The twist angle is reduced accordingly. These results demonstrate that a linear thickness variation produces twist results that are comparable to the base model results.

A more realistic braid material model consists of high modulus carbon fibers in one weave direction combined with low modulus glass fibers in the other weave direction. The low modulus fibers are required to produce the final 2D weave. These low modulus fibers do not need to have the same volume fraction as the carbon fibers, and can be tailored to produce the maximum bend-twist coupling. Figure 21 illustrates the variation in twist angle and coupling coefficient depending on the glass fiber to carbon fiber volume fraction ratio. The results for 1.00 are for equal volume fractions; the results for 0.80 are for 80% glass fibers to 100% carbon fibers. More twist and a higher coupling coefficient are produced by using the lower volume fraction ratio of 0.80.

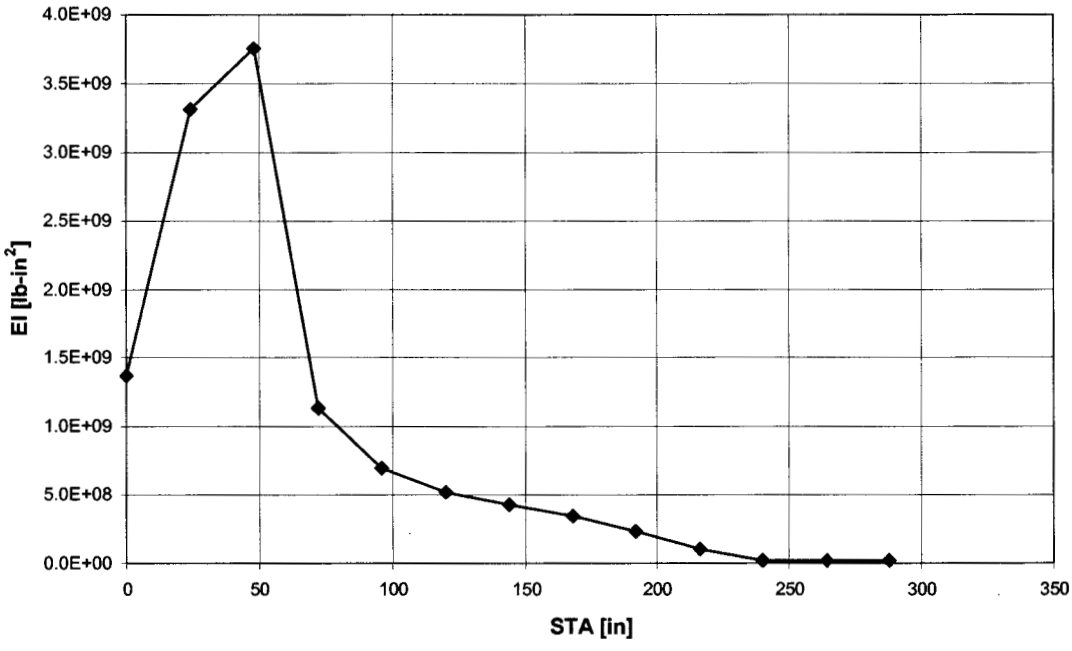

Figure 13: SERI-8 bending stiffness [3]

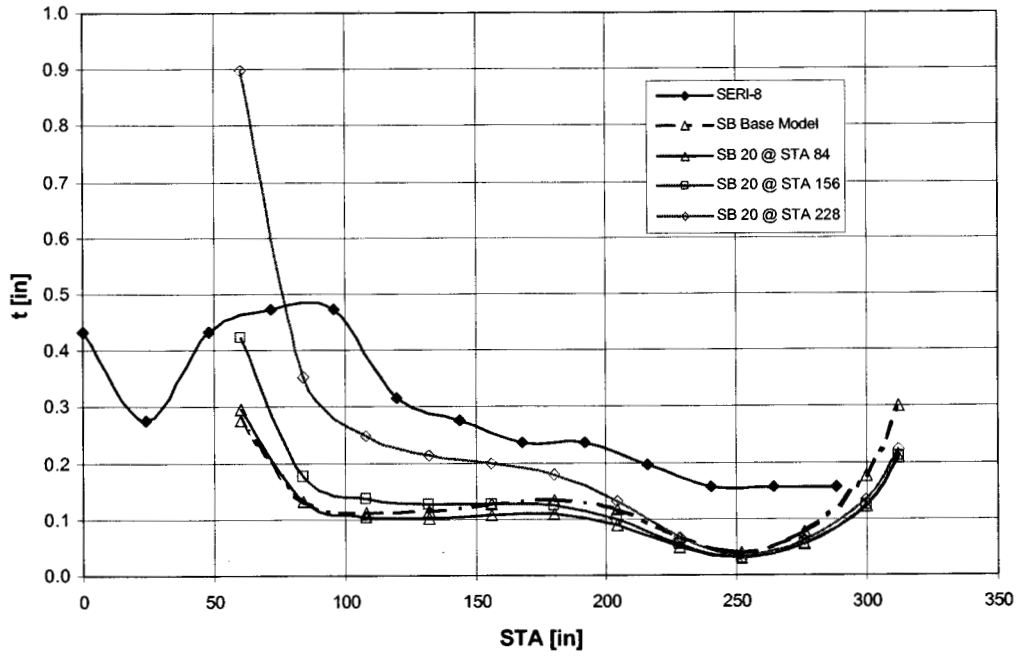

Figure 14a: Double box required thickness

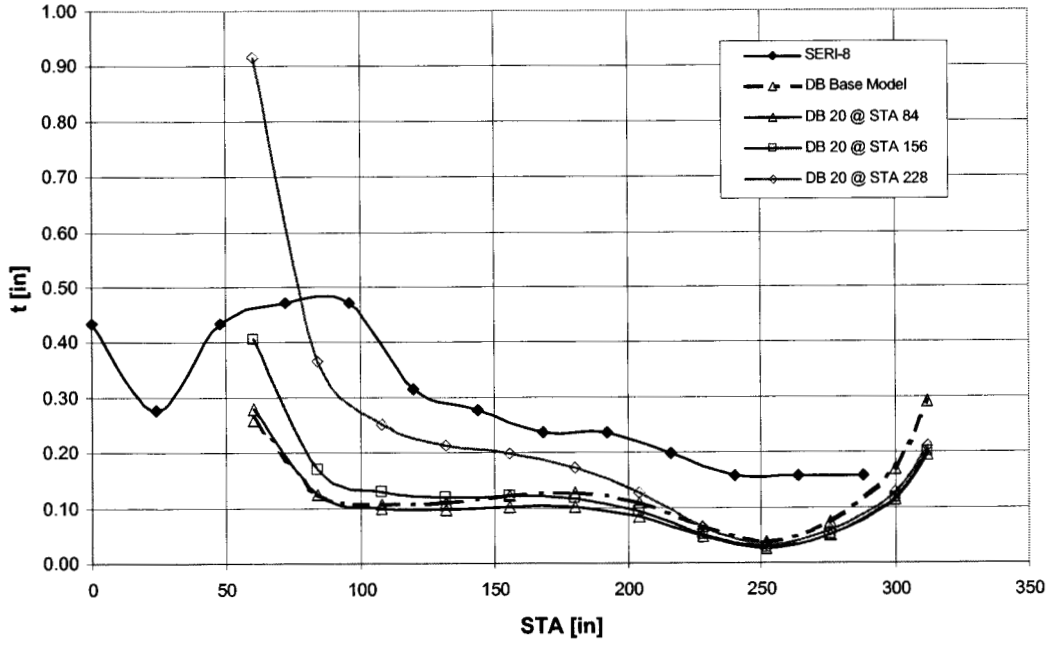

Figure 14b: Single box required thickness

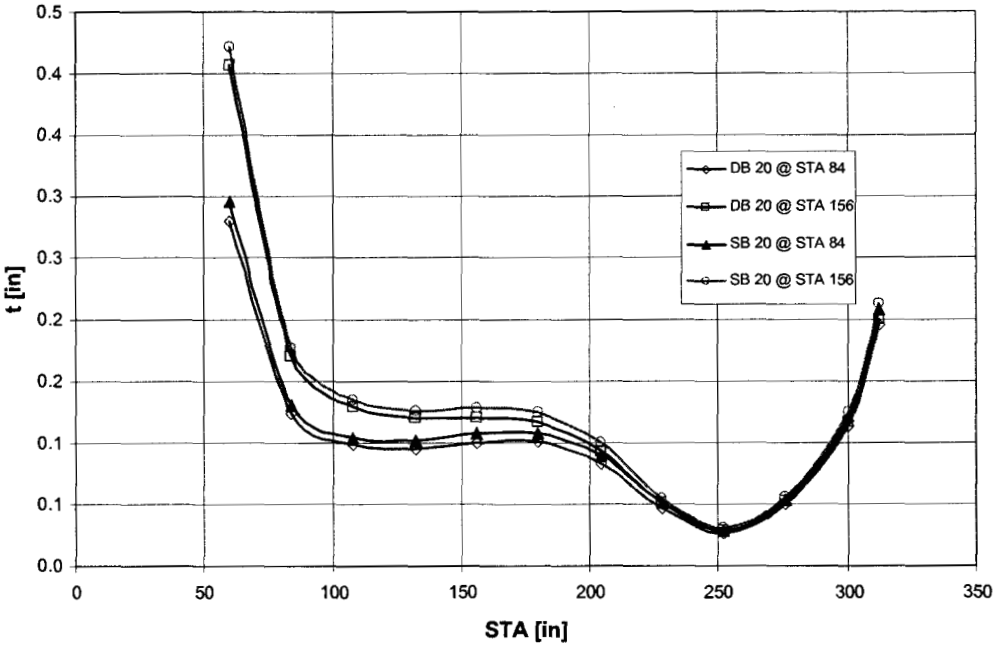

Figure 15: Comparison of double box and single box thickness

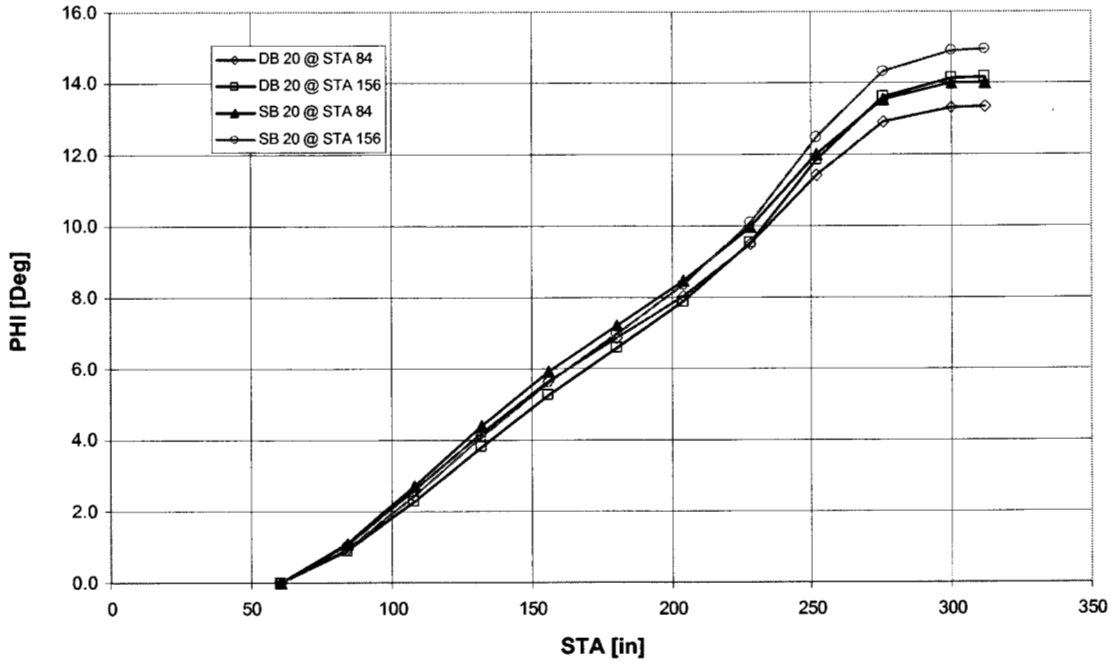

Figure 16a: Comparison of double box and single box twist angle

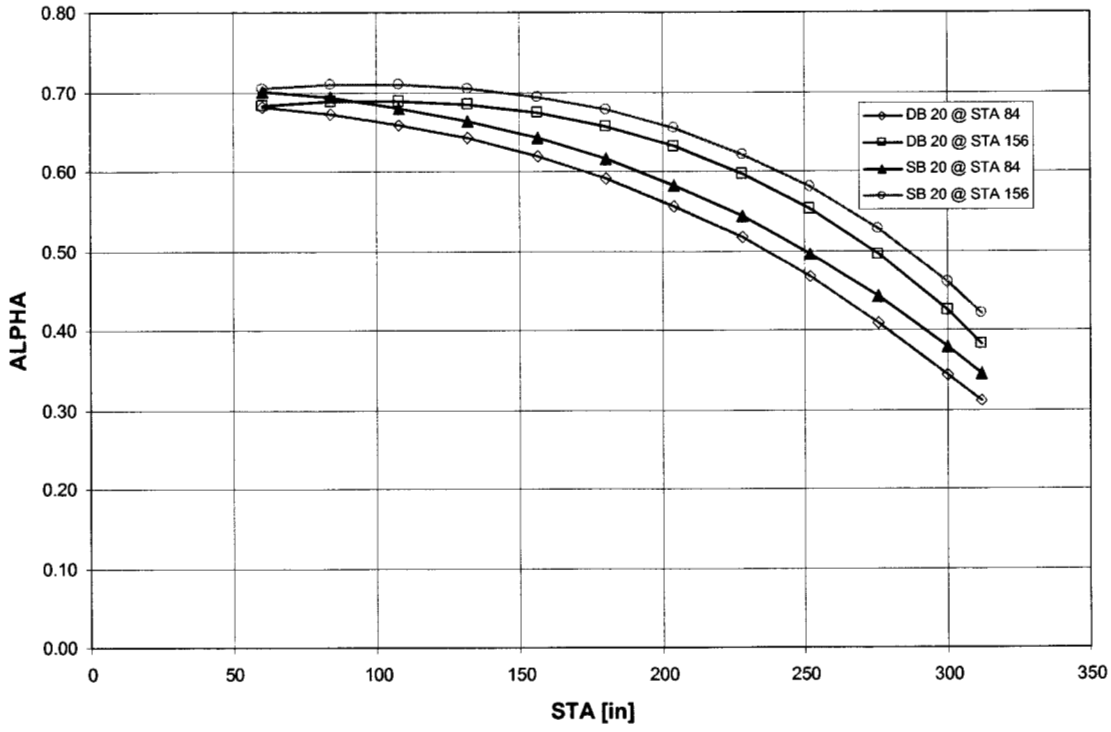

Figure 16b: Comparison of double box and single box coupling coefficient

Figure 17a: Comparison of double box and single box maximum shear flow

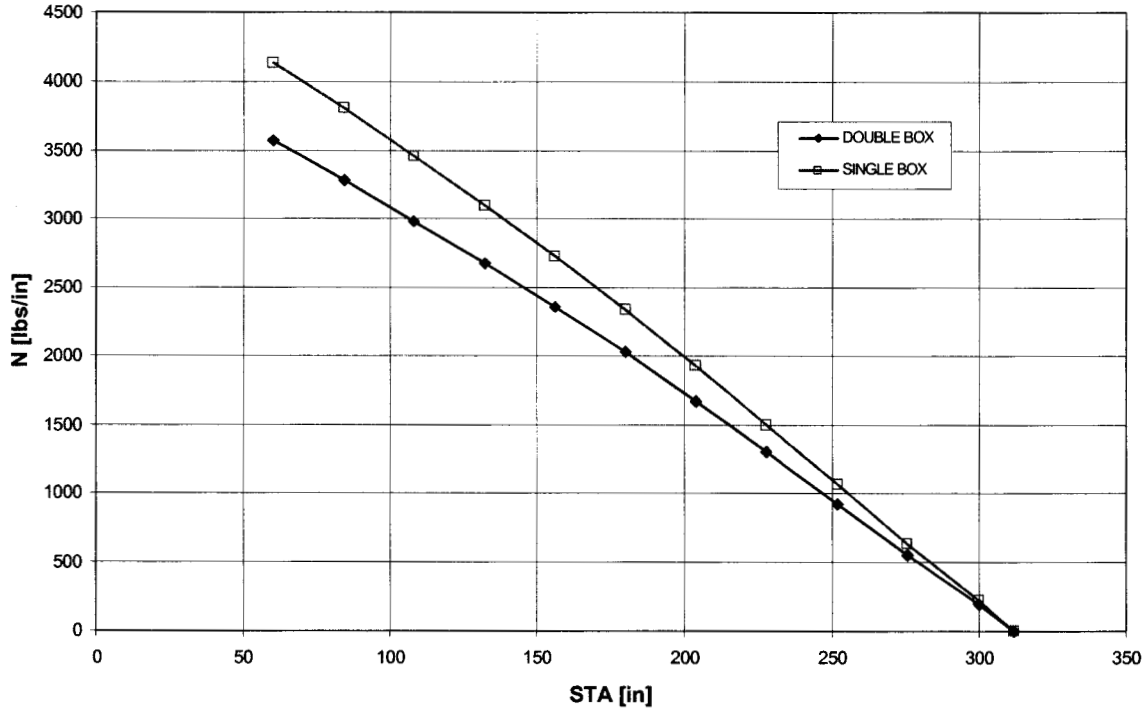

Figure 17b: Comparison of double box and single box maximum axial force

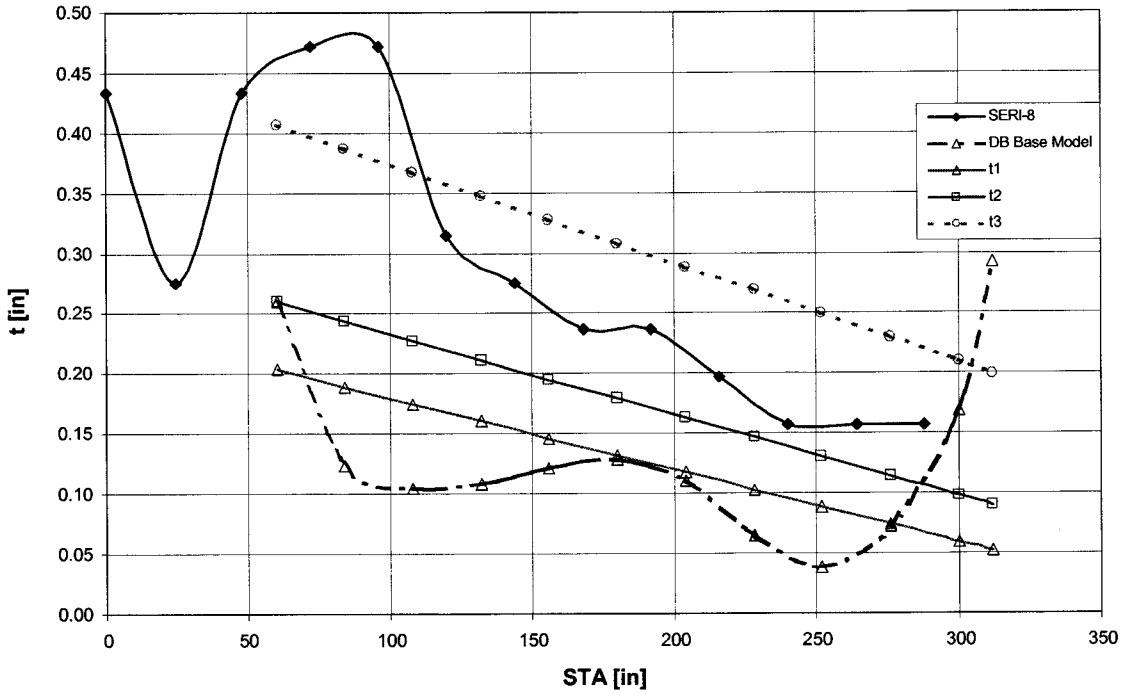

Figure 18: Linear thickness variations

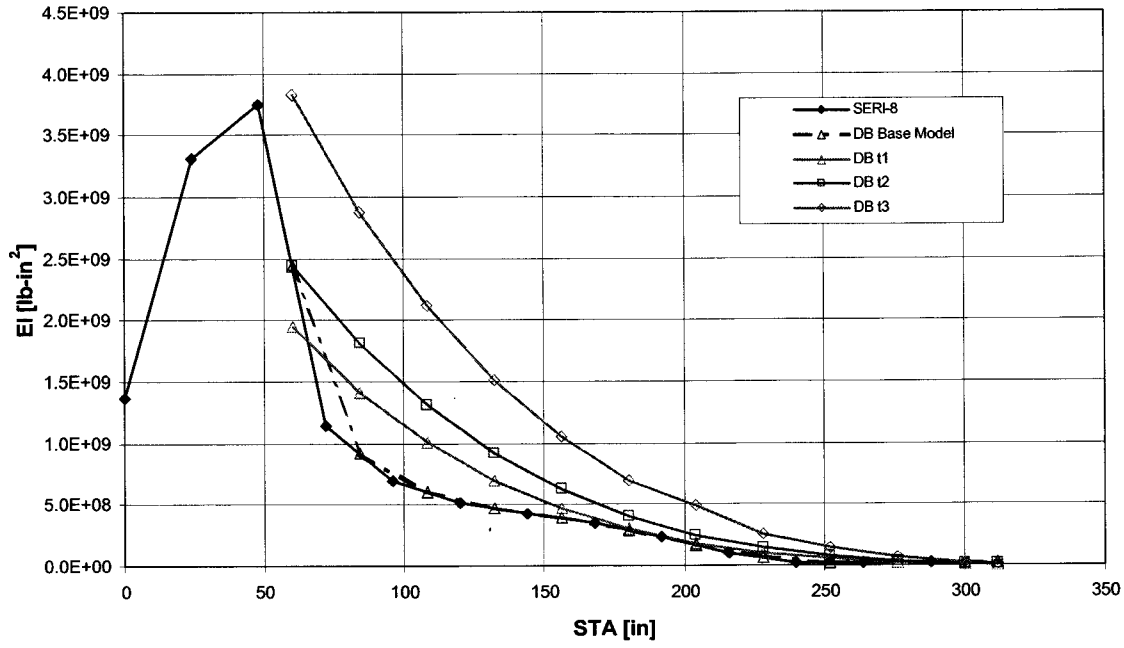

Figure 19: Bending stiffness for linear thickness variations

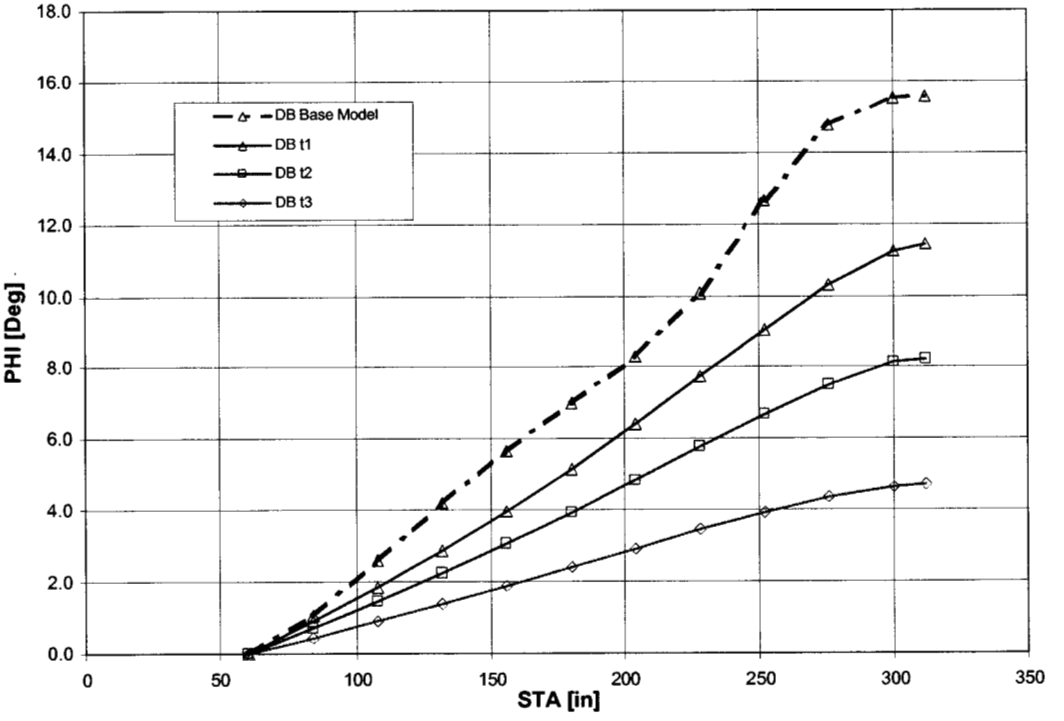

Figure 20: Twist angle for linear thickness variations

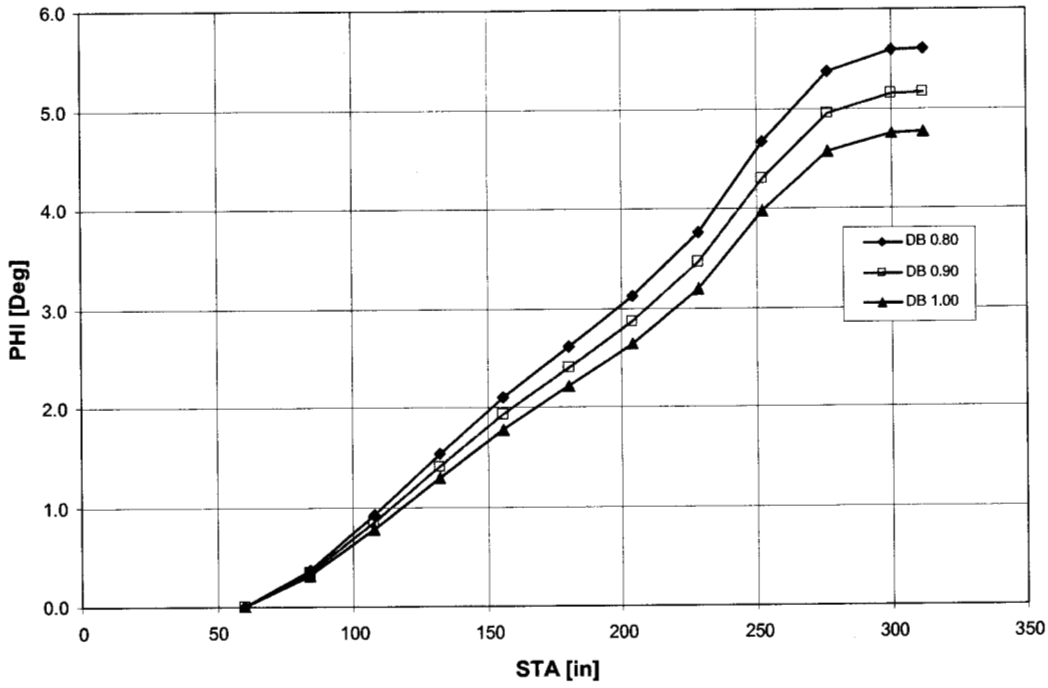

Figure 21a: Double box twist angle with carbon/glass weave

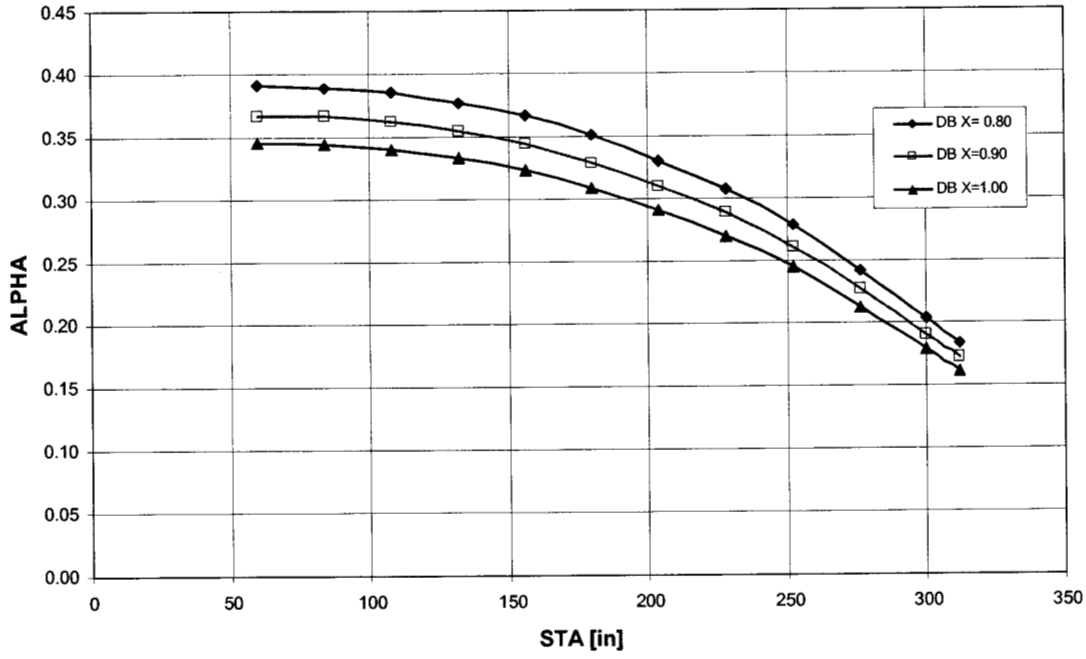

Figure 21b: Double box coupling coefficient with carbon/glass weave

7 FINAL DESIGN

As previously noted, undulating thickness variations would be very difficult (and undesirable) to manufacture, and a more efficient design is achieved if a few continuous layers of material are used. For the final design, three possible variations in thickness were studied as shown in Figure 22. These thickness variations were combined with the realistic braid material model consisting of high modulus carbon fibers and low modulus glass fibers. The glass fiber to carbon fiber volume fraction ratio is assumed to be 0.80.

Results for the stiffness, twist and coupling coefficient corresponding to the three thickness variations are shown in Figures 23 and 24. Tabulated design results are given in Tables 4 through 6. Final layer arrangements are tabulated in Table 7 and illustrated in Figures 25 through 27. Relative weight values are shown in Figures 28 and 29. These values do not include the resin weight. For the three designs, design 2 (the t2 thickness variation) is judged to be the most favorable. The bending stiffness and thickness are practically identical to those of the base model, which was sized to match the SERI-8 stiffness. The twist and coupling coefficient are also comparable to the base model, and can be improved for the final design (as required) by using either a lower glass fiber to carbon fiber volume fraction ratio or a lower stiffness glass fiber. The relative weight of design 2 is also modest compared to design 1, and it is very close to the weight of design 3.

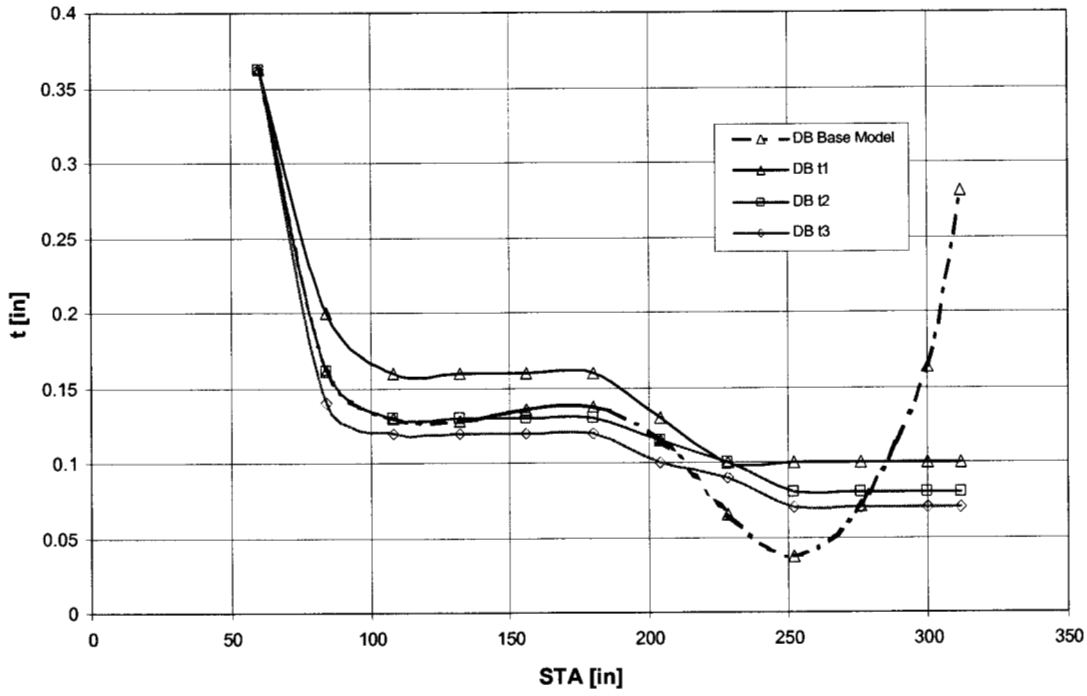

Figure 22: Proposed thickness variations for final design

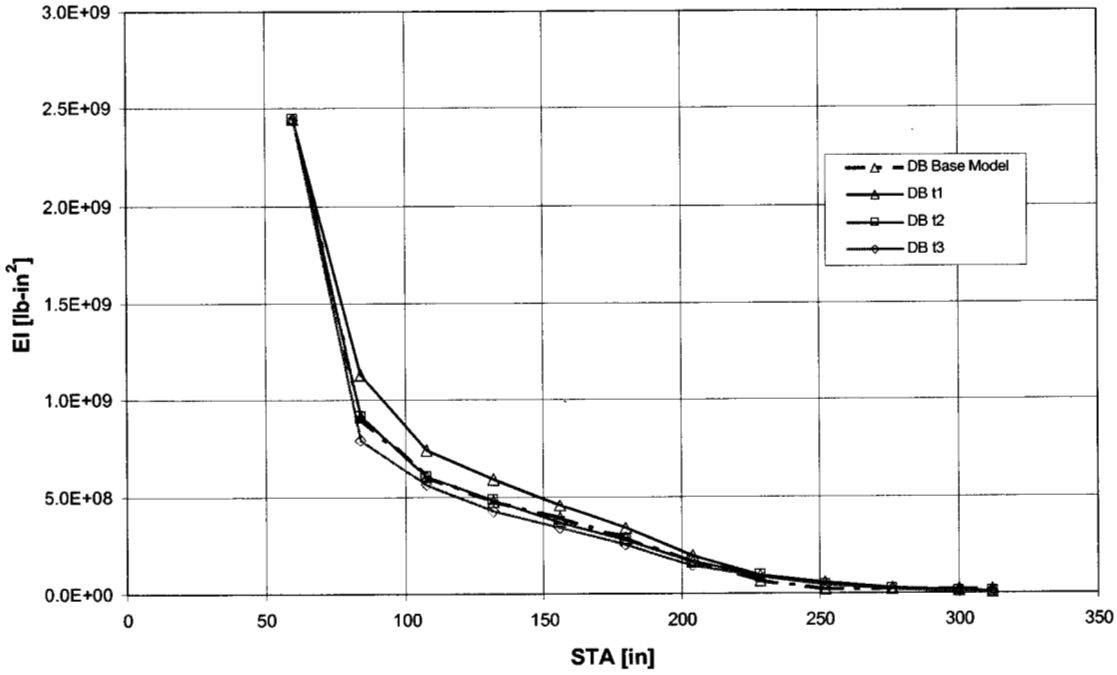

Figure 23: Bending stiffness variations for proposed thickness variations

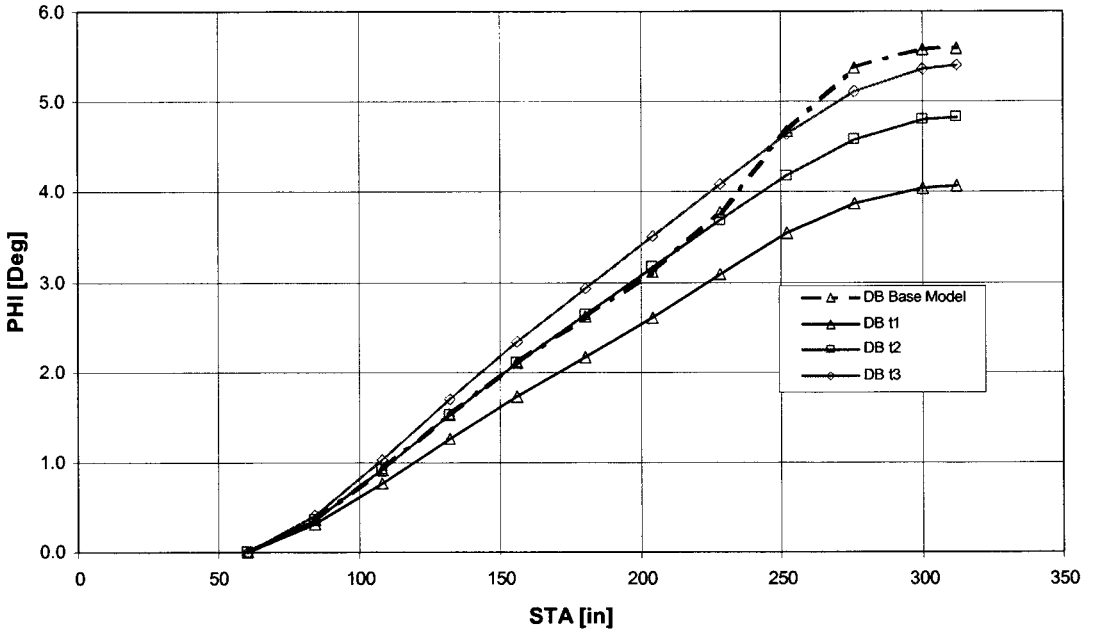

Figure 24a: Twist angle variations for proposed thickness variations

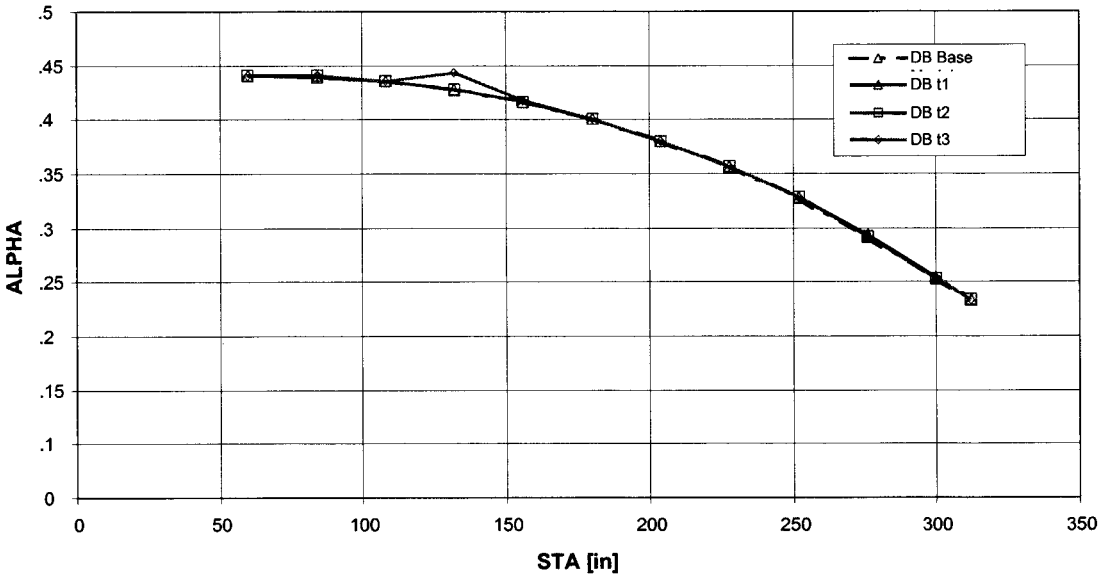

Figure 24b: Coupling coefficient for proposed thickness variations

DOUBLE BOX DESIGN CONCEPT (HYBRID 20 Deg @ STA 84)
t1

Mechanical response

Properties	60	84	108	132	156	180	204	228	252	276	300	312
Angle [Deg]	21.60	**20.00**	18.40	16.80	15.30	13.70	12.10	10.60	9.10	7.50	6.00	5.30
Thickness Carbon [in]	0.2014	0.1111	0.0889	0.0889	0.0889	0.0889	0.0722	0.0556	0.0556	0.0556	0.0556	0.0556
Thickness Glass [in]	0.1611	0.0889	0.0711	0.0711	0.0711	0.0711	0.0578	0.0444	0.0444	0.0444	0.0444	0.0444
Thickness Lay-up [in]	0.3625	0.2000	0.1600	0.1600	0.1600	0.1600	0.1300	0.1000	0.1000	0.1000	0.1000	0.1000
E*Iyy [lb*in^2]	244.500E+07	113.500E+07	74.540E+07	59.370E+07	45.540E+07	33.620E+07	19.140E+07	9.653E+07	5.796E+07	3.072E+07	1.329E+07	7.711E+06
Offset [%]	0	-24	-23	-25	-18	-16	-13	-52	-166	-41	39	64
G*J [lb*in^2]	120.000E+07	49.560E+07	28.950E+07	20.560E+07	14.210E+07	9.413E+07	4.842E+07	2.243E+07	12.530E+06	6.260E+06	2.642E+06	1.540E+06
Density (ρ) [lb/in^3]	0.0647	0.0647	0.0647	0.0647	0.0647	0.0647	0.0647	0.0647	0.0647	0.0647	0.0647	0.0647
Relative Weight (W) [lb]	29.383	15.260	11.326	10.405	9.483	8.561	6.231	4.235	3.659	3.083	2.507	2.219
Total Weight (W) [lb]	106.353	106.353	106.353	106.353	106.353	106.353	106.353	106.353	106.353	106.353	106.353	106.353
Coupling Coefft. (α)	0.391	0.389	0.385	0.377	0.366	0.351	0.330	0.307	0.278	0.243	0.204	0.184
Stiffness Term. (g)	66.940E+07	29.210E+07	17.890E+07	13.180E+07	9.320E+07	6.237E+07	3.177E+07	14.280E+06	7.503E+06	3.363E+06	1.208E+06	6.349E+05

Torsional reponse

	60	84	108	132	156	180	204	228	252	276	300	312
Flexibility Term (Z)	2.692E-10	6.119E-10	9.733E-10	1.259E-09	1.664E-09	2.247E-09	3.848E-09	7.279E-09	1.120E-08	1.858E-08	3.589E-08	5.533E-08
Moment (Mx)	61.320E+04	48.330E+04	37.170E+04	27.750E+04	19.950E+04	13.650E+04	8.730E+04	5.070E+04	2.550E+04	9900	2100	0.00
Rate of Twist (Z*Mx)	1.651E-04	2.957E-04	3.618E-04	3.494E-04	3.320E-04	3.067E-04	3.359E-04	3.690E-04	2.856E-04	1.839E-04	75.369E-06	0.00
Incremental Twist Angle ($\Delta\phi$)	5.53E-03	7.89E-03	8.53E-03	8.18E-03	7.66E-03	7.71E-03	8.46E-03	7.86E-03	5.63E-03	3.11E-03	4.52E-04	
Twist Angle (ϕ) [Rad]	0.0000	0.0055	0.0134	0.0220	0.0301	0.0378	0.0455	0.0540	0.0618	0.0675	0.0706	0.0710
Twist Angle (ϕ) [Deg]	0.00	0.32	0.77	1.26	1.73	2.17	2.61	3.09	3.54	3.86	4.04	4.07

Internal Loading

	60	84	108	132	156	180	204	228	252	276	300	312
Shear Flow [q]	203.069	189.700	175.411	160.566	146.347	128.311	110.146	89.582	67.691	43.650	16.230	0.00
Axial Force [N]	3390.000	3129.000	2854.000	2566.000	2263.000	1940.000	1600.000	1242.000	877.131	513.360	182.534	0.00

Table 4: Properties of the double box, 20 degrees @ STA 84, thickness t1

DOUBLE BOX DESIGN CONCEPT (HYBRID 20 Deg @ STA 84)
t2

Mechanical response

Properties	60	84	108	132	156	180	204	228	252	276	300	312
Angle [Deg]	21.60	**20.00**	18.40	16.80	15.30	13.70	12.10	10.60	9.10	7.50	6.00	5.30
Thickness Carbon [in]	0.2014	0.0897	0.0724	0.0724	0.0724	0.0724	0.0638	0.0556	0.0444	0.0444	0.0444	0.0444
Thickness Glass [in]	0.1611	0.0717	0.0579	0.0579	0.0579	0.0579	0.0510	0.0444	0.0356	0.0356	0.0356	0.0356
Thickness Lay-up [in]	0.3625	0.1614	0.1303	0.1303	0.1303	0.1303	0.1148	0.1000	0.0800	0.0800	0.0800	0.0800
E*Iyy [lb*in^2]	244.500E+07	91.650E+07	60.700E+07	48.350E+07	37.090E+07	27.380E+07	16.900E+07	9.653E+07	4.633E+07	2.455E+07	1.062E+07	6.162E+06
Offset [%]	0	0	0	-2	4	5	0	-52	-113	-13	51	72
G*J [lb*in^2]	120.000E+07	40.000E+07	23.580E+07	16.740E+07	11.570E+07	7.666E+07	4.277E+07	2.243E+07	10.020E+06	5.005E+06	2.112E+06	1.232E+06
Density (ρ) [lb/in^3]	0.0647	0.0647	0.0647	0.0647	0.0647	0.0647	0.0647	0.0647	0.0647	0.0647	0.0647	0.0647
Relative Weight (W) [lb]	29.383	12.354	9.248	8.497	7.747	6.996	5.513	4.235	2.937	2.477	2.016	1.785
Total Weight (W) [lb]	93.187	93.187	93.187	93.187	93.187	93.187	93.187	93.187	93.187	93.187	93.187	93.187
Coupling Coefft. (α)	0.391	0.390	0.385	0.377	0.366	0.351	0.330	0.307	0.278	0.242	0.203	0.184
Stiffness Term. (g)	66.940E+07	23.590E+07	14.570E+07	10.730E+07	7.590E+07	5.080E+07	2.809E+07	14.280E+06	5.986E+06	2.683E+06	9.634E+05	5.065E+05

Torsional reponse

	60	84	108	132	156	180	204	228	252	276	300	312
Flexibility Term (Z)	2.692E-10	7.587E-10	1.195E-09	1.546E-09	2.043E-09	2.760E-09	4.360E-09	7.279E-09	1.397E-08	2.319E-08	4.480E-08	6.907E-08
Moment (Mx)	61.320E+04	48.330E+04	37.170E+04	27.750E+04	19.950E+04	13.650E+04	8.730E+04	5.070E+04	2.550E+04	9900	2100	0.00
Rate of Twist (Z*Mx)	1.651E-04	3.667E-04	4.442E-04	4.290E-04	4.076E-04	3.767E-04	3.806E-04	3.690E-04	3.562E-04	2.296E-04	94.080E-06	0.00
Incremental Twist Angle (Δϕ)	6.38E-03	9.73E-03	1.05E-02	1.00E-02	9.41E-03	9.09E-03	9.00E-03	8.70E-03	7.03E-03	3.88E-03	5.64E-04	
Twist Angle (ϕ) [Rad]	0.0000	0.0064	0.0161	0.0266	0.0366	0.0460	0.0551	0.0641	0.0728	0.0799	0.0837	0.0843
Twist Angle (ϕ) [Deg]	0.00	0.37	0.92	1.52	2.10	2.64	3.16	3.67	4.17	4.58	4.80	4.83

Internal Loading

	60	84	108	132	156	180	204	228	252	276	300	312
Shear Flow [q]	203.069	189.700	175.411	160.566	146.347	128.311	110.146	89.582	67.691	43.650	16.230	0.00
Axial Force [N]	3390.000	3129.000	2854.000	2566.000	2263.000	1940.000	1600.000	1242.000	876.976	513.268	182.504	0.00

Table 5: Properties of the double box, 20 degrees @ STA 84, thickness t2

DOUBLE BOX DESIGN CONCEPT (HYBRID 20 Deg @ STA 84)
t3

Mechanical response

Properties	60	84	108	132	156	180	204	228	252	276	300	312
Angle [Deg]	21.60	**20.00**	18.40	16.80	15.30	13.70	12.10	10.60	9.10	7.50	6.00	5.30
Thickness Carbon [in]	0.2014	0.0778	0.0667	0.0667	0.0667	0.0667	0.0556	0.0500	0.0389	0.0389	0.0389	0.0389
Thickness Glass [in]	0.1611	0.0622	0.0533	0.0533	0.0533	0.0533	0.0444	0.0400	0.0311	0.0311	0.0311	0.0311
Thickness Lay-up [in]	0.3625	0.1400	0.1200	0.1200	0.1200	0.1200	0.1000	0.0900	0.0700	0.0700	0.0700	0.0700
E*Iyy [lb*in^2]	244.500E+07	79.490E+07	55.910E+07	42.560E+07	34.160E+07	25.220E+07	14.730E+07	8.684E+07	4.056E+07	2.150E+07	9.299E+06	5.396E+06
Offset [%]	0	13	8	10	12	13	13	-37	-86	1	57	75
G*J [lb*in^2]	120.000E+07	34.690E+07	21.720E+07	16.260E+07	10.660E+07	7.061E+07	3.726E+07	2.018E+07	8.771E+06	4.382E+06	1.849E+06	1.078E+06
Density (ρ) [lb/in^3]	0.0647	0.0647	0.0647	0.0647	0.0647	0.0647	0.0647	0.0647	0.0647	0.0647	0.0647	0.0647
Relative Weight (W) [lb]	29.383	10.734	8.524	7.833	7.142	6.451	4.812	3.817	2.575	2.171	1.768	1.566
Total Weight (W) [lb]	86.777	86.777	86.777	86.777	86.777	86.777	86.777	86.777	86.777	86.777	86.777	86.777
Coupling Coefft. (α)	0.391	0.390	0.385	0.393	0.367	0.351	0.330	0.307	0.278	0.242	0.204	0.184
Stiffness Term. (g)	66.940E+07	20.460E+07	13.430E+07	10.340E+07	6.994E+07	4.681E+07	2.448E+07	12.830E+06	5.248E+06	2.352E+06	8.447E+05	4.441E+05

Torsional reponse

	60	84	108	132	156	180	204	228	252	276	300	312
Flexibility Term (Z)	2.692E-10	8.746E-10	1.298E-09	1.767E-09	2.219E-09	2.998E-09	5.008E-09	8.081E-09	1.599E-08	2.653E-08	5.126E-08	7.902E-08
Moment (Mx)	61.320E+04	48.330E+04	37.170E+04	27.750E+04	19.950E+04	13.650E+04	8.730E+04	5.070E+04	2.550E+04	9900	2100	0.00
Rate of Twist (Z*Mx)	1.651E-04	4.227E-04	4.825E-04	4.903E-04	4.427E-04	4.092E-04	4.372E-04	4.097E-04	4.077E-04	2.626E-04	1.076E-04	0.00
Incremental Twist Angle (Δϕ)	7.05E-03	1.09E-02	1.17E-02	1.12E-02	1.02E-02	1.02E-02	1.02E-02	9.81E-03	8.04E-03	4.44E-03	6.46E-04	
Twist Angle (ϕ) [Rad]	0.0000	0.0071	0.0179	0.0296	0.0408	0.0510	0.0612	0.0713	0.0811	0.0892	0.0936	0.0943
Twist Angle (ϕ) [Deg]	0.00	0.40	1.03	1.70	2.34	2.92	3.50	4.09	4.65	5.11	5.36	5.40

Internal Loading

	60	84	108	132	156	180	204	228	252	276	300	312
Shear Flow [q]	203.069	189.700	175.411	160.566	146.347	128.311	110.146	89.582	67.691	43.650	16.601	0.00
Axial Force [N]	3390.000	3129.000	2854.000	2564.000	2263.000	1940.000	1600.000	1242.000	877.086	513.334	182.828	0.00

Table 6: Properties of the double box, 20 degrees @ STA 84, thickness t3

FINAL DESIGN DOUBLE BOX LAYER ARRANGEMENT

20 Deg @ STA 84 t1

	60	84	108	132	156	180	204	228	252	276	300	312
Proposed Thickness (t1) [in]	0.3625	0.2000	0.1600	0.1600	0.1600	0.1600	0.1300	0.1000	0.1000	0.1000	0.1000	0.1000
Carbon Thickness [in]	0.2014	0.1111	0.0889	0.0889	0.0889	0.0889	0.0722	0.0556	0.0556	0.0556	0.0556	0.0556
Glass Thickness [in]	0.1611	0.0889	0.0711	0.0711	0.0711	0.0711	0.0578	0.0444	0.0444	0.0444	0.0444	0.0444
Theoretical Number of Socks	18.5410	9.5997	7.1570	6.6170	6.0615	5.4920	3.9896	2.6985	2.3221	1.9408	1.5553	1.3613
Practical Number of Socks	19	10	8	7	7	6	4	3	3	2	2	2
New Thickness (t1R) [in]	0.3715	0.2083	0.1788	0.1693	0.1848	0.1748	0.1303	0.1112	0.1292	0.1031	0.1286	0.1469

20 Deg @ STA 84 t2

	60	84	108	132	156	180	204	228	252	276	300	312
Proposed Thickness (t2) [in]	0.3625	0.1614	0.1303	0.1303	0.1303	0.1303	0.1148	0.1000	0.0800	0.0800	0.0800	0.0800
Carbon Thickness [in]	0.2014	0.0897	0.0724	0.0724	0.0724	0.0724	0.0638	0.0556	0.0444	0.0444	0.0444	0.0444
Glass Thickness [in]	0.1611	0.0717	0.0579	0.0579	0.0579	0.0579	0.0510	0.0444	0.0356	0.0356	0.0356	0.0356
Theoretical Number of Socks	18.5410	7.7470	5.8285	5.3887	4.9363	4.4726	3.5231	2.6985	1.8577	1.5526	1.2443	1.0890
Practical Number of Socks	19	8	6	6	5	5	4	3	2	2	2	2
New Thickness (t2R) [in]	0.3715	0.1667	0.1341	0.1451	0.1320	0.1457	0.1303	0.1112	0.0861	0.1031	0.1286	0.1469

20 Deg @ STA 84 t3

	60	84	108	132	156	180	204	228	252	276	300	312
Proposed Thickness (t3) [in]	0.3625	0.1400	0.1200	0.1200	0.1200	0.1200	0.1000	0.0900	0.0700	0.0700	0.0700	0.0700
Carbon Thickness [in]	0.2014	0.0778	0.0667	0.0667	0.0667	0.0667	0.0556	0.0500	0.0389	0.0389	0.0389	0.0389
Glass Thickness [in]	0.1611	0.0622	0.0533	0.0533	0.0533	0.0533	0.0444	0.0400	0.0311	0.0311	0.0311	0.0311
Theoretical Number of Socks	18.5410	6.7198	5.3677	4.9627	4.5461	4.1190	3.0689	2.4286	1.6255	1.3586	1.0887	0.9529
Practical Number of Socks	19	7	6	5	5	5	4	3	2	2	2	1
New Thickness (t3R) [in]	0.3715	0.1458	0.1341	0.1209	0.1320	0.1457	0.1303	0.1112	0.0861	0.1031	0.1286	0.0735

Table 7: Final design layer arrangement

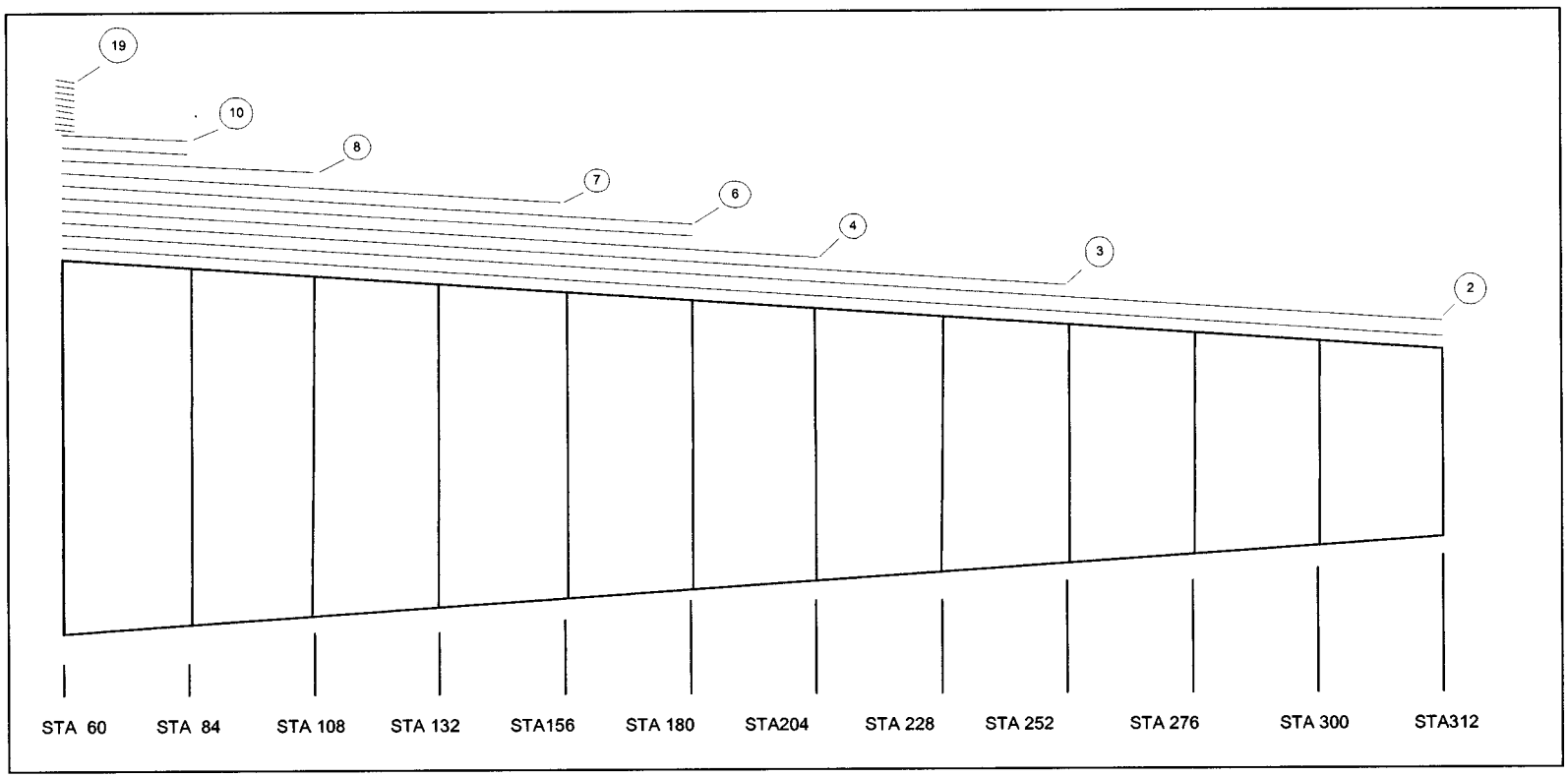

Figure 25: Sock arrangement, 20 degrees @ STA 84, thickness t1

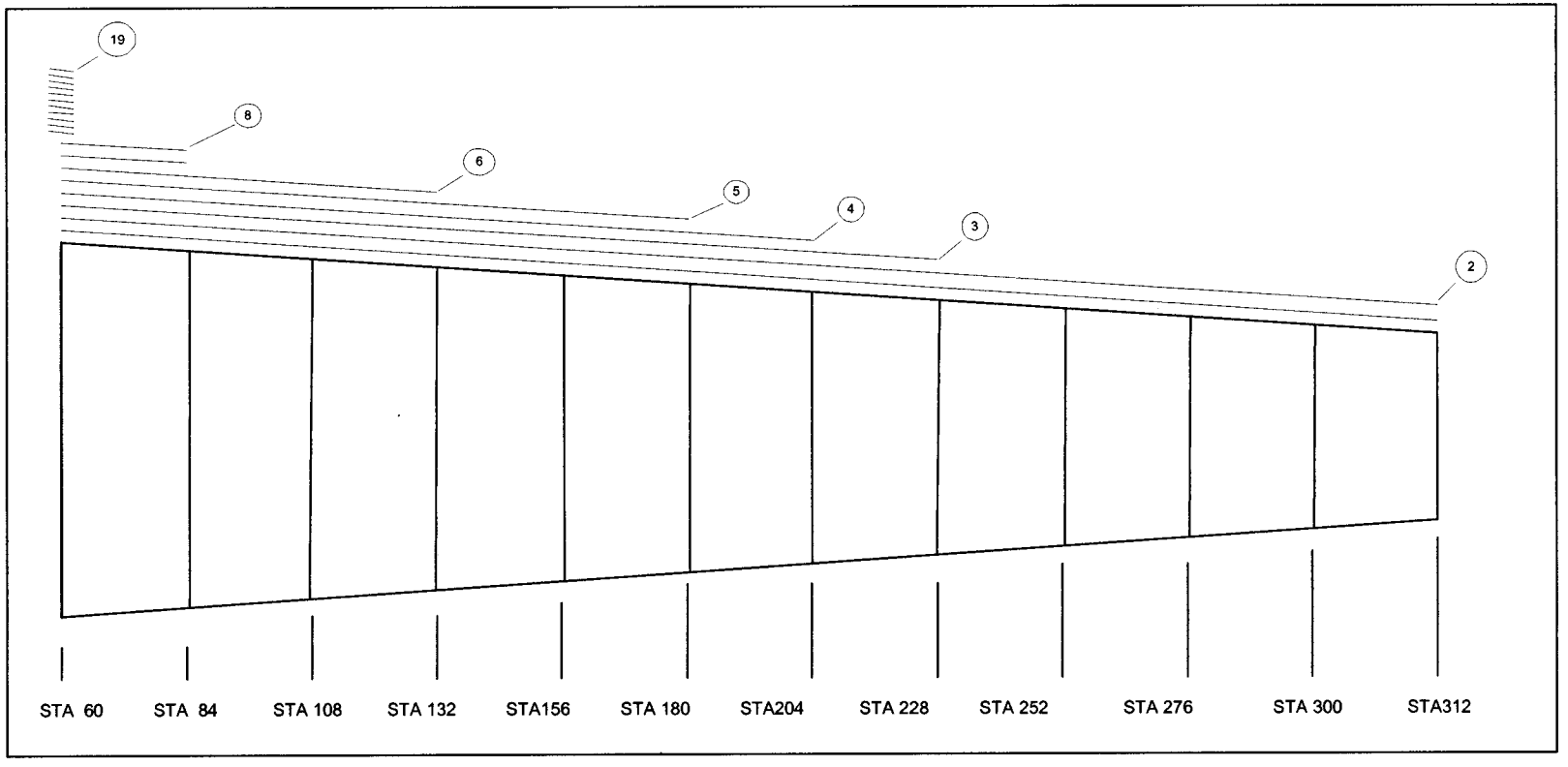

Figure 26: Sock arrangement, 20 degrees @ STA 84, thickness t2

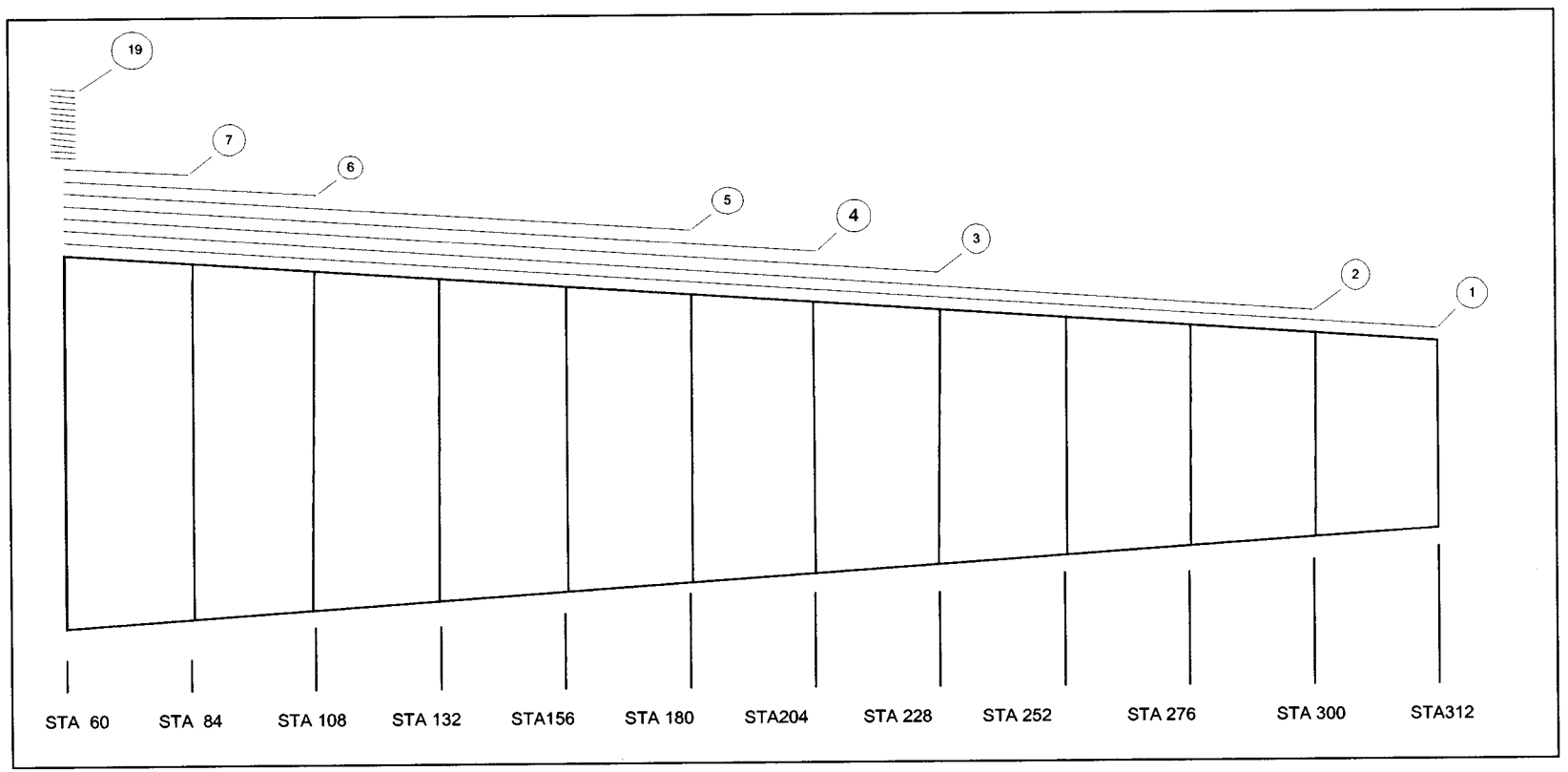

Figure 27: Sock arrangement, 20 degrees @ STA 84, thickness t3

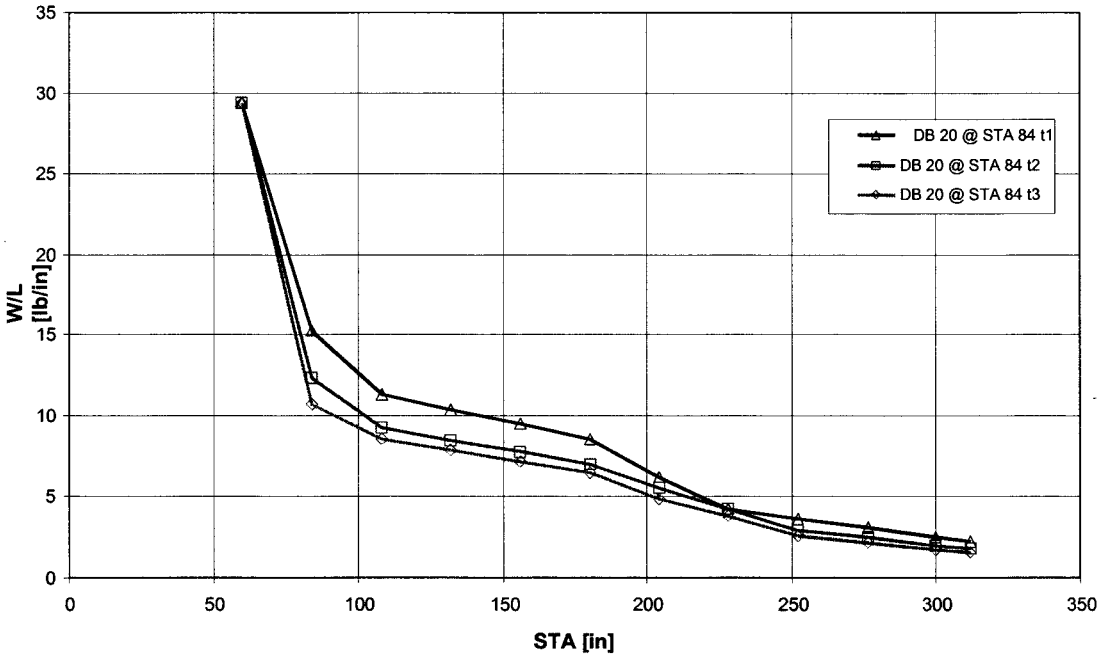

Figure 28: Relative weight distribution, resin not included

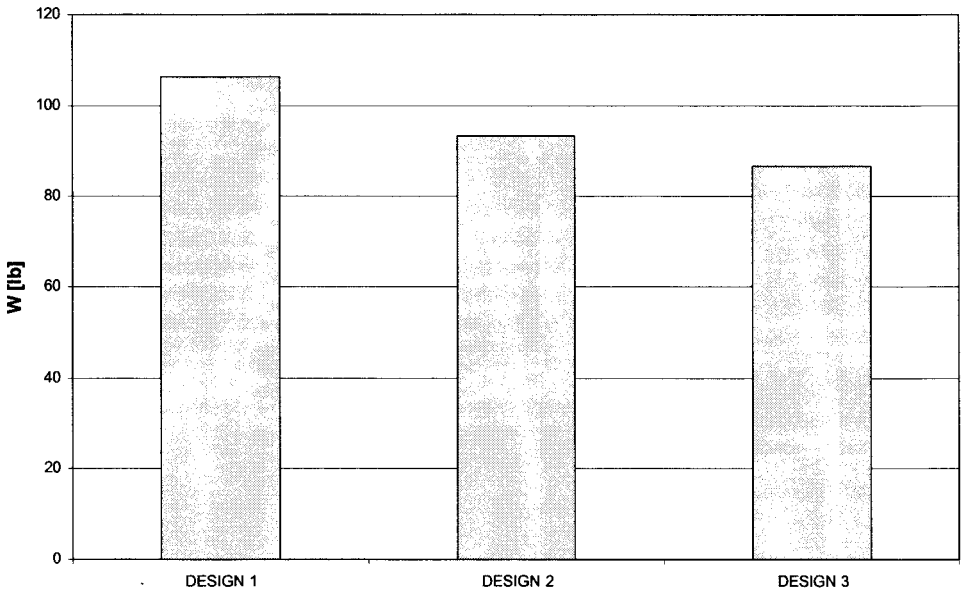

Figure 29: Total weight, resin not included

8 FINITE ELEMENT RESULTS

The beam theory presented in Section 5 of this report has been used as a basis for all results. This section presents finite element twist results for the double box design 2 (the t2 thickness variation from Table 5). The model was constructed using MSC/NASTRAN quadrilateral elements with appropriate laminated stiffness properties. The model mesh and geometry are shown in Figure 30. Figure 31 shows the comparison between finite element and beam theory results. The difference between the finite element and beam theory results is judged to be reasonable. Similar differences were obtained by Chandra, Stemple and Chopra [8]. The beam model does not account for end restraints that prevent warping; whereas, the finite element model is fully restrained for all degrees-of-freedom at the root. Further studies are required to completely document the differences between finite element and beam theory results. A comparison with finite element results was included in this report only as a means of evaluating the relative accuracy of the beam theory.

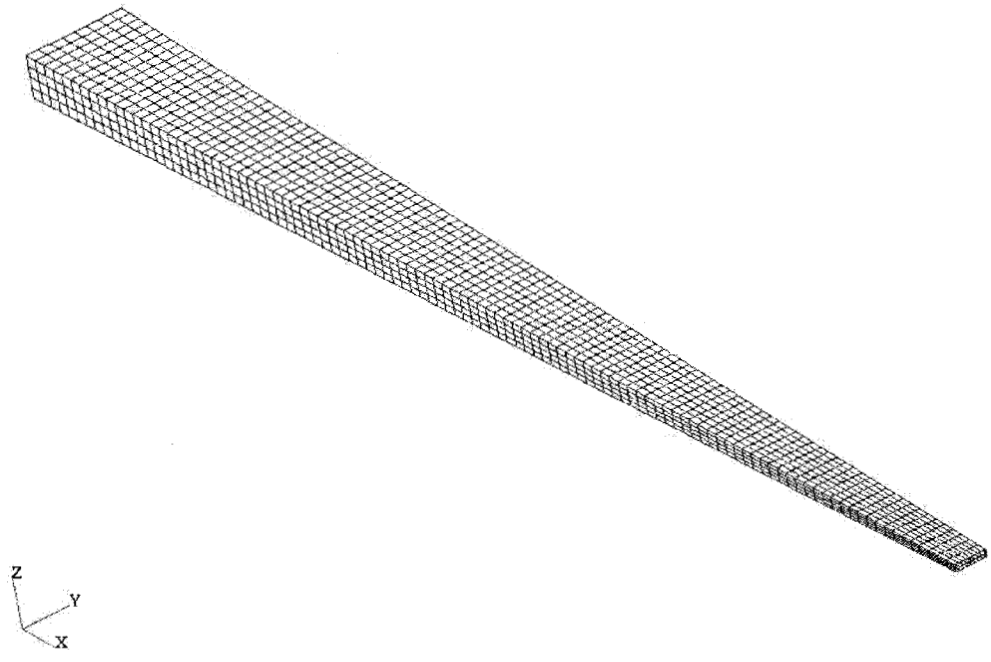

Figure 30 Finite element model mesh and geometry

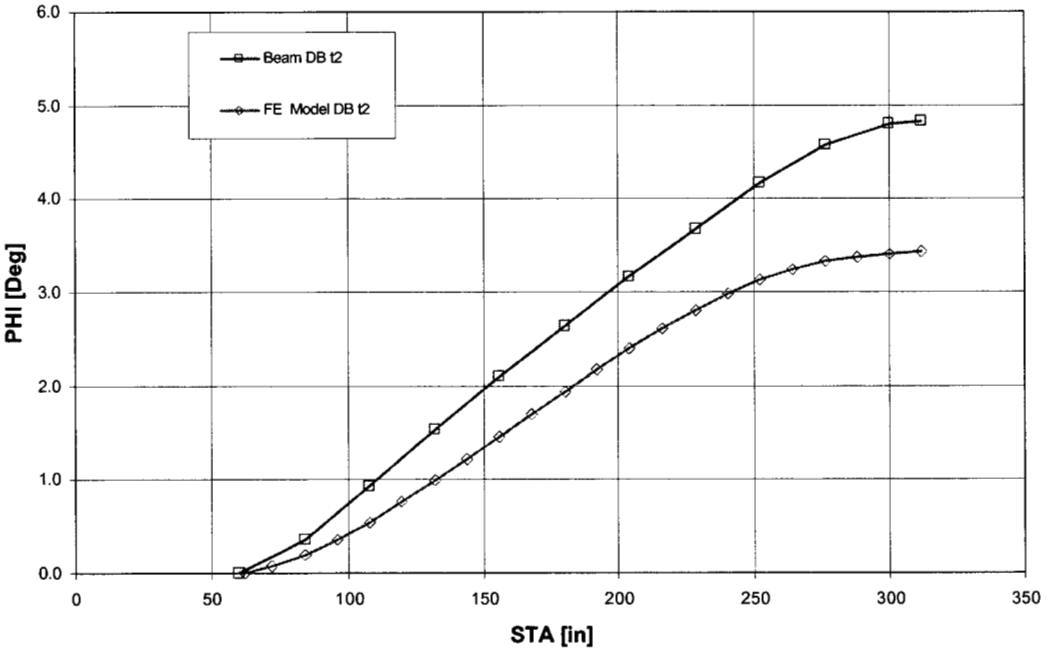

Figure 31 Comparison of finite element and beam theory twist angle variations

9 CONCLUSIONS

The results of this study indicate that a braided composite blade can be designed with the required stiffness properties and structural coupling. The braid angle and the geometrical properties are the most important parameters that govern the mechanical behavior of the structure. Due to the box taper, the braid angle varies with blade span. Parametric results indicate that the best results can be achieved using a braid angle of 20 degrees @ blade STA 84. It was shown that bend-twist coupling can be increased by reducing the glass fiber volume fraction, which also reduces the structural weight. A volume fraction ratio of 80% was chosen for the final design. A double box configuration shows the best behavior in terms of the shear flow and the internal axial force; consequently, lower stresses (and strains) are produced under a bending load. The double box also provides additional structural redundancy, which is desirable for safety and fatigue.

All of the results for this study were determined based on the blade geometry and stiffness of the SERI-8 [3]. The stiffness at STA 60 is dominated by the fitting stiffness, which is very high compared to the blade stiffness. This results in a large number of layers at STA 60. Future detailed design studies should consider an integral design where the blade and the root fitting are both manufactured using braided preforms. This would eliminate stiffness discontinuities at the blade-fitting interface and should result in a more efficient structure.

REFERENCES

1. N.K. Naik, *Woven Fabric Composites*, Technomic Publishing Company, 1994.

2. W.C. de Goeij, M.J.L. van Tooren, and A. Beukers, "Implementation of Bending-Torsion Coupling in the Design of a Wind-Turbine Rotor-Blade," *Applied Energy*, Vol. 63, 1999, pp. 191-207.

3. C.H. Ong and S.W. Tsai, "The Use of Carbon Fibers in Wind Turbine Blade Design: a SERI-8 Blade Example," SAND2000-0478, Sandia National Laboratories, Albuquerque, NM, March 2000.

4. B.N. Cox and G. Flanagan, *Handbook of Analytical Methods for Textile Composites*, NASA CR-4750.

5. C.H. Ong and S.W. Tsai, "Design, Manufacture and Testing of a Bend-Twist D-Spar," SAND99-1324, Sandia National Laboratories, Albuquerque, NM, June 1999.

6. C. Libove, "Stresses and Rate of Twist in Single-Cell Thin-Walled Beams with Anisotropic Walls," *AIAA Journal*, Vol. 26, No. 9, Sept. 1998, pp. 1107-1118.

7. D.W. Lobitz, P.S. Veers, G.R. Eisler, D.J. Laino, P.G. Migliore, and G. Bir, "The Use of Twist-Coupled Blades to Enhance the Performance of Horizontal Axis Wind Turbines," SAND2001-1003, Sandia National Laboratories, Albuquerque, NM, May 2001.

8. R. Chandra, A.D. Stemple, and I. Chopra, "Thin-Walled Composite Beams Under Bending, Torsional, and Extensional Loads," *AIAA Journal of Aircraft*, Vol. 27, No. 7, July 1990, pp. 619-626.

DISTRIBUTION

H. Ashley
Dept. of Aeronautics and
Astronautics Mechanical Engr.
Stanford University
Stanford, CA 94305

K. Bergey
University of Oklahoma
Aero Engineering Department
Norman, OK 73069

D. Berry
TPI Composites Inc.
373 Market Street
Warren, RI 02885

R. Blakemore
GE Wind
13681 Chantico Road
Tehachapi, CA 93561

C. P. Butterfield
NREL
1617 Cole Boulevard
Golden, CO 80401

G. Bywaters
Northern Power Systems
Box 999
Waitsfield,VT 05673

J. Cadogan
Office of Wind and Hydro Technology
EE-12
U.S. Department of Energy
1000 Independence Avenue SW
Washington, DC 20585

D. Cairns
Montana State University
Mechanical & Industrial Engineering Dept.
220 Roberts Hall
Bozeman, MT 59717

S. Calvert
Office of Wind and Hydro Technology
EE-12
U.S. Department of Energy
1000 Independence Avenue SW
Washington, DC 20585

J. Chapman
OEM Development Corp.
840 Summer St.
Boston, MA 02127-1533

Kip Cheney
PS Enterprises
222 N. El Segundo, #576
Palm Springs, CA 92262

C. Christensen, Vice President
GE Wind
13681 Chantico Road
Tehachapi, CA 93561

R. N. Clark
USDA
Agricultural Research Service
P.O. Drawer 10
Bushland, TX 79012

C. Cohee
Foam Matrix, Inc.
1123 East Redondo Blvd.
Inglewood, CA 90302

J. Cohen
Princeton Economic Research, Inc.
1700 Rockville Pike
Suite 550
Rockville, MD 20852

C. Coleman
Northern Power Systems
Box 999
Waitsfield, VT 05673

K. J. Deering
The Wind Turbine Company
515 116th Avenue NE
No. 263
Bellevue, WA 98004

A. J. Eggers, Jr.
RANN, Inc.
744 San Antonio Road, Ste. 26
Palo Alto, CA 94303

D. M. Eggleston
DME Engineering
1605 W. Tennessee Ave.
Midland, TX 79701-6083

P. R. Goldman
Director
Office of Wind and Hydro Technology
EE-12
U.S. Department of Energy
1000 Independence Avenue SW
Washington, DC 20585

D. Griffin
GEC
5729 Lakeview Drive NE, Ste. 100
Kirkland, WA 98033

C. Hansen
Windward Engineering
4661 Holly Lane
Salt Lake City, UT 84117

C. Hedley
Headwaters Composites, Inc.
PO Box 1073
Three Forks, MT 59752

S. Hock
Wind Energy Program
NREL
1617 Cole Boulevard
Golden, CO 80401

D. Hodges
Georgia Institute of Technology
270 Ferst Drive
Atlanta, GA 30332

Bill Holley
3731 Oakbrook
Pleasanton, CA 94588

K. Jackson
Dynamic Design
123 C Street
Davis, CA 95616

E. Jacobsen
GE Wind
13000 Jameson Rd.
Tehachapi, CA 93561

G. James
University of Houston
Dept. of Mechanical Engineering
4800 Calhoun
Houston, TX 77204-4792

M. Kramer
Foam Matrix, Inc.
PO Box 6394
Malibu CA 90264

A. Laxson
NREL
1617 Cole Boulevard
Golden, CO 80401

S. Lockard
TPI Composites Inc.
373 Market Street
Warren, RI 02885

J. Locke, Associate Professor (5)
Wichita State University
207 Wallace Hall, Box 44
Wichita, KS 67620-0044

D. Malcolm
GEC
5729 Lakeview Drive NE, Ste. 100
Kirkland, WA 98033

J. F. Mandell
Montana State University
302 Cableigh Hall
Bozeman, MT 59717

T. McCoy
GEC
5729 Lakeview Drive NE, Ste. 100
Kirkland, WA 98033

L. McKittrick
Montana State University
Mechanical & Industrial Engineering Dept.
220 Roberts Hall
Bozeman, MT 59717

P. Migliore
NREL
1617 Cole Boulevard
Golden, CO 80401

A. Mikhail
Clipper Windpower Technology, Inc.
7985 Armas Canyon Road
Goleta, CA 93117

W. Musial
NREL
1617 Cole Boulevard
Golden, CO 80401

NWTC Library (5)
NREL
1617 Cole Boulevard
Golden, CO 80401

B. Neal
USDA
Agricultural Research Service
P.O. Drawer 10
Bushland, TX 79012

V. Nelson
Department of Physics
West Texas State University
P.O. Box 248
Canyon, TX 79016

T. Olsen
Tim Olsen Consulting
1428 S. Humboldt St.
Denver, CO 80210

R. Z. Poore, President
Global Energy Concepts, Inc.
5729 Lakeview Drive NE
Suite 100
Kirkland, WA 98033

R. G. Rajagopalan
Aerospace Engineering Department
Iowa State University
404 Town Engineering Bldg.
Ames, IA 50011

J. Richmond
MDEC
3368 Mountain Trail Ave.
Newbury Park, CA 91320

Michael Robinson
NREL
1617 Cole Boulevard
Golden, CO 80401

D. Sanchez
U.S. Dept. of Energy
Albuquerque Operations Office
P.O. Box 5400
Albuquerque, NM 87185

R. Sherwin
Atlantic Orient
PO Box 1097
Norwich, VT 05055

Brian Smith
NREL
1617 Cole Boulevard
Golden, CO 80401

J. Sommer
Molded Fiber Glass Companies/West
9400 Holly Road
Adelanto, CA 93201

K. Starcher
AEI
West Texas State University
P.O. Box 248
Canyon, TX 79016

F. S. Stoddard
79 S. Pleasant St. #2A
Amherst, MA 01002

A. Swift
University of Texas at El Paso
320 Kent Ave.
El Paso, TX 79922

J. Thompson
ATK Composite Structures
PO Box 160433
MS YC14
Clearfield, UT 84016-0433

R. W. Thresher
NREL
1617 Cole Boulevard
Golden, CO 80401

S. Tsai
Stanford University
Aeronautics & Astronautics
Durand Bldg. Room 381
Stanford, CA 94305-4035

W. A. Vachon
W. A. Vachon & Associates
P.O. Box 149
Manchester, MA 01944

C. P. van Dam
Dept of Mech and Aero Eng.
University of California, Davis
One Shields Avenue
Davis, CA 95616-5294

B. Vick
USDA, Agricultural Research Service
P.O. Drawer 10
Bushland, TX 79012

K. Wetzel
K. Wetzel & Co., Inc.
PO Box 4153
4108 Spring Hill Drive
Lawrence, KS 66046-1153

R. E. Wilson
Mechanical Engineering Dept.
Oregon State University
Corvallis, OR 97331

M. Zuteck
MDZ Consulting
601 Clear Lake Road
Clear Lake Shores, TX 77565

M.S. 0557	T. J. Baca, 9125
M.S. 0557	T. G. Carne, 9124
M.S. 0708	H. M. Dodd, 6214 (25)
M.S. 0708	T. D. Ashwill, 6214 (10)
M.S. 0708	D. E. Berg, 6214
M.S. 0708	R. R. Hill, 6214
M.S. 0708	P. L. Jones 6214
M.S. 0708	D. L. Laird, 6214
M.S. 0708	D. W. Lobitz, 6214
M.S. 0708	M. A. Rumsey, 6214
M.S. 0708	H. J. Sutherland, 6214
M.S. 0708	P. S. Veers, 6214
M.S. 0708	J. Zayas, 6214
M.S. 0847	K. E. Metzinger, 9126
M.S. 0958	M. Donnelly, 14172
M.S. 1490	A. M. Lucero, 12660
M.S. 0612	Review & Approval Desk, 9612 For DOE/OSTI
M.S. 0899	Technical Library, 9616 (2)
M.S. 9018	Central Technical Files, 8945-1